CHAPTER 5

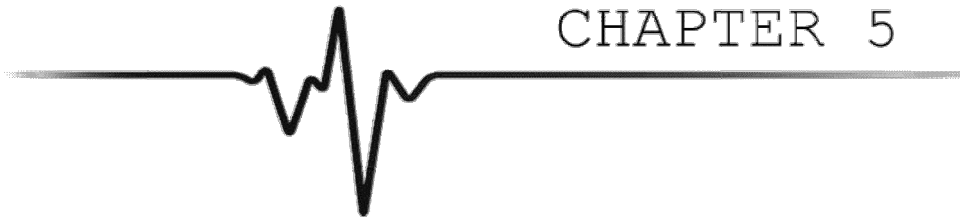

CHAPTER 5

SEISMIC ANISOTROPY IN THE CRUST

5.1 INTRODUCTION

Seismic waves are sensitive to elastic properties of the earth and hence study of seismic waves is considered as the most prominent approach to investigate the earth's structure. While travelling through from the source to recording site, seismic waves carry information of propagating medium all along its travel path. One of the physical properties of a medium affecting the speed of a seismic wave is the seismic anisotropy. It is a unique property of underlying rocks/foliated formations which affect the passage of seismic waves leading to directional dependence of seismic wave velocity causing seismic anisotropy (Babuška & Cara, 1991; Savage, 1999). When a shear wave propagates through an anisotropic medium, it splits into fast and slow polarized S-waves with different velocities (Fig. 5.1). This phenomenon is referred to as shear wave splitting (Crampin, 1981; Babuška & Cara, 1991; Savage, 1999). This mechanism is the elastic analogue of the birefringence phenomenon observed in polarized microscopy technique. The polarization direction of the fast S-wave is termed as fast polarization direction (FPD) (Φ) and the time difference between the fast and slow split waves is called delay time (δt). The FPD shows the orientation of anisotropy and delay time provides an estimate of the strength of anisotropy. Both these parameters are useful for characterizing seismic anisotropy in the propagating medium.

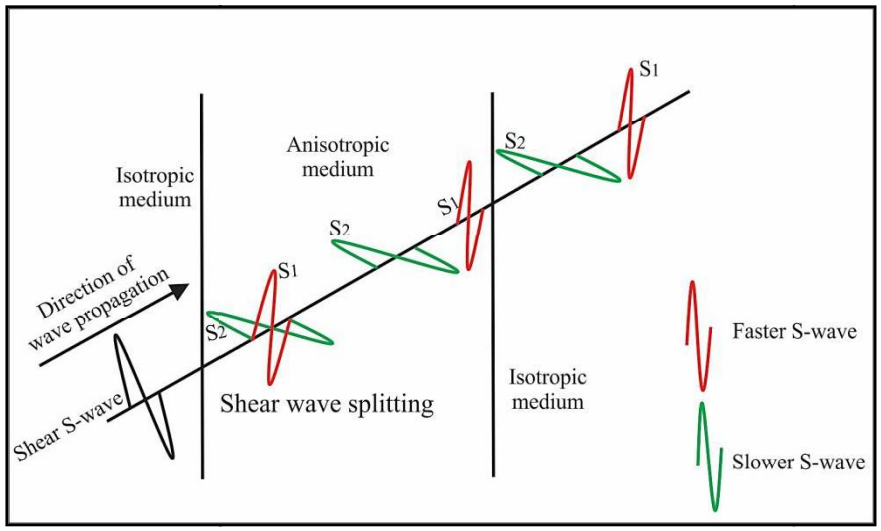

Figure 5.1 Shear wave splitting of S-wave into two orthogonally polarised fast and slow shear waves propagating in an anisotropic medium.

Seismic anisotropy is a ubiquitous characteristic of the earth's crust, mantle and inner core and splitting of shear waves is the most explicit sign of seismic anisotropy observed at different layers of the earth. The origin of anisotropy can be distinct in nature for each layer of the earth. The upper most part of the earth-crust possesses cracks, joints, layers of bedded sedimentary or foliated metamorphic rocks. The anisotropy in the crust is originated by aligned micro-cracks which is known as shape preferred orientation (SPO) developed due to tectonic stress and/or due to the alignment of intrinsic anisotropic minerals of rocks, referred as lattice preferred orientation (LPO) (Meissner et al., 2006). The upper crust is probably dominated by crack related (Crampin & Peacock, 2008), whereas middle-to-lower crust is expected to be chiefly influenced by the LPO (Barruol & Mainprice, 1993). The anisotropic minerals in the lower crust are aligned due to tectonics stresses and deformation. The seismic anisotropy is particularly related to the lithological and physical properties of rocks. Additionally, mechanical properties like rock fabric, cracks and foliations resulted frc

A number of seismic anisotropy studies have been carried out in the Himalaya-Tibetan orogeny particularly in Tibetan Plateau to study the anisotropy in the crust (Ozacar et al., 2004; Sherrington et al., 2004; Sun et al., 2012; Chen et al., 2013; Yang et al., 2015; Wu et al., 2015; Cai et al., 2016; Paul et al., 2017) and upper mantle (e.g. McNamara et al., 1994; Hirn et al., 1995; Sandvol et al., 1997; Huang, 2000; Herquel & Tapponnier, 2005; Lev et al., 2006; Singh et al., 2007; Kumar & Singh, 2008; Heintz et al., 2009; Hazarika et al., 2013). The studies related to crustal anisotropy are very limited in the NW Himalaya. Seismic anisotropy study carried out by Heintz et al. (2009) concluded that seismic anisotropy in the southern Indian shield is NNE–SSW oriented FPDs that becomes nearly E-W in the Himalaya. Oreshin et al. (2008) also studied anisotropy in the upper mantle beneath western LKZ. A recent study by Paul et al. (2017) discussed the crustal anisotropy in the Trans-Himalayan (Eastern Ladakh) region and reported the considerable strength of crustal anisotropy with FPD oriented along the strike of the Karakorum Fault. Most of the RF studies carried out in the NW Himalaya did not emphasize on the possible presence of crustal anisotropy and considered the subsurface structure as composed of horizontally stratified homogeneous isotropic layer during RF inversion (Rai et al., 2006; Oreshin et al., 2008, 2011; Hazarika et al., 2014).

Laboratory experiments have also been performed to study the anisotropic properties of rocks at room pressure and temperature (P-T) conditions in the Himalaya (Gogte & Ramana, 1982; Gupta, 2009; Sharma et al., 2011; Sharma, 2011; Gupta & Sharma, 2012; Tandon & Gupta, 2015). Gupta, (2009) studied the seismic velocity characteristics of Higher Himalayan rocks of Satluj valley and yielded the anisotropic behavior of such rocks. Sharma et al. (2011) studied seismic and petrophysical characteristics of Himalayan granitoid and inferred that the variations of the seismic velocities are controlled by the preferred orientation of minerals.

The study area is one of the most complex geological sections of the Himalayas which cut through the major litho-tectonic units of the Himalaya along the Satluj River. The northern part of the study area is characterised by several normal and thrust faults obtained through field data and focal

mechanism solution of earthquakes (Molanr & Lyon-Cean, 1989; Burchfiel et al., 1992; McCaffrey & Nabelek, 1998; Hogdes et al., 2001; Thiede et al., 2006; Yadav et al., 2017). Source of information on the crustal deformation and existing stress can also be obtained by inversion of focal mechanism solutions (Gephart & Forsyth, 1984; Michael, 1987). However, due to uncertainty in the true fault plane from two nodal planes, this method alone cannot provide reliable information.

In this chapter, the relationship between tectonic stresses/deformation and anisotropic behaviour of the crust is studied using Moho converted *Ps* phases clearly observable in RFs of teleseismic earthquakes recorded beneath the Satluj valley. In addition, laboratory measurements of compressional and shear wave velocities of rock samples collected from lithological units of Satluj valley has been investigated at room pressure and temperature conditions. This shear wave splitting study provides important insight about the crustal deformation of the whole crust owing to tectonic stresses which have significant implication in understanding geodynamic evolution of the study region.

5.2 THEORETICAL BACKGROUND

A seismic wave is a type of elastic wave that travels within the earth and contains all the necessary information of both source and properties of the medium through which they propagate. The polarization of seismic wave mainly depends on three factors viz. (a) types of wave, (b) path of propagating wave and (c) elastic properties of the medium. In order to understand the propagation of elastic waves, it is required to study the mechanism of deformation and functional forces in an elastic medium.

If any external force or stress is applied on the elastic solid medium, it will deform the size and shape of the medium. The particles of elastic solid will try to acquire their original position when the external force is withdrawn. The propagation of seismic waves is associated with the projection of their propagation direction of the elastic tensor in anisotropic medium (Aki & Richards, 1980). The elastic behaviour of an anisotropic medium can be

represented by a set of elastic constants defined over a range of an anisotropic symmetric system.

Suppose, an elastic solid block on which a stress σ_{ij} is applied as a force acting on a particular plane with components of normal (with similar indices) and shear stresses (with different indices) in a j^{th} direction defining the state of stress at a point (Fig. 5.2).

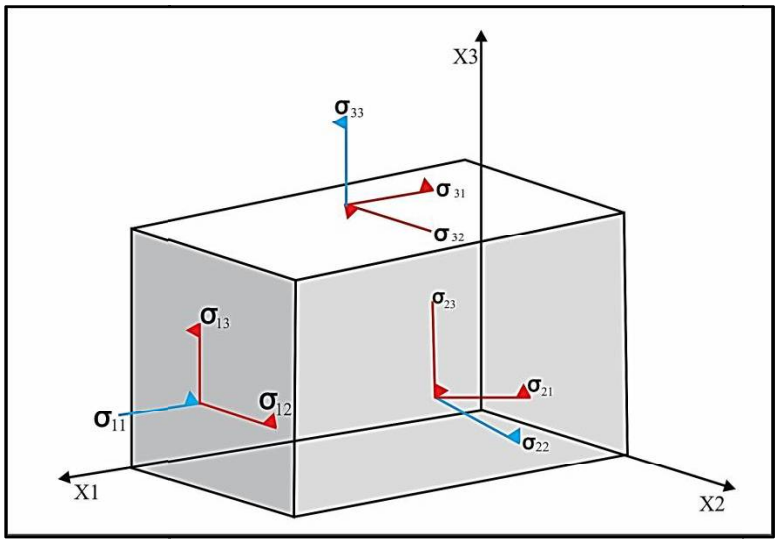

Figure 5.2 A schematic representation of stresses acting on a solid elastic block with normal and shear stresses.

The force applied on a solid elastic medium is defined as stress tensor, σij and deformation take place due to applied force are described as strain tensor, ϵ_{ij}.

$$\sigma ij = \begin{pmatrix} \sigma_{11} & \sigma_{12} & \sigma_{13} \\ \sigma_{21} & \sigma_{22} & \sigma_{23} \\ \sigma_{31} & \sigma_{23} & \sigma_{33} \end{pmatrix} \text{ and } \epsilon_{ij} = \begin{pmatrix} \epsilon_{11} & \epsilon_{12} & \epsilon_{13} \\ \epsilon_{21} & \epsilon_{22} & \epsilon_{23} \\ \epsilon_{31} & \epsilon_{23} & \epsilon_{33} \end{pmatrix} \text{where i, j= 1,2,3}$$

In the elastic wave theory, the relationship between the external forces/stresses and deformation/strain is defined by famous physicist Robert Hooke in 1660 as Hooke's law. According to Hooke's law, the strain produced in an elastic medium is directly proportional to applied stress acting within the elastic limits of the medium. Mathematically, it can be expressed as:

$$\sigma_{ij} = C_{ijkl}\epsilon_{kl}$$

where i, j, k, l = 1, 2, 3 and σ_{ij} is second rank stress tensor; C_{ijkl} is stiffness tensor and ϵ_{kl} is the strain tensor of a solid elastic medium. If the medium exhibits the symmetrical properties, then $\sigma_{ij} = \sigma_{ji}$; $\epsilon_{ij} = \epsilon_{ji}$ and this property makes stiffness tensor also symmetric

i.e. $$C_{ijkl} = C_{ijlk}; C_{ijkl} = C_{jikl} \quad (5.2)$$

The elastic properties in a medium behave differently in different directions and this kind of property makes a medium anisotropic. To evaluate the symmetrical properties of the medium, it is required to study the Hooke's law with the concept of thermodynamics. The elastic stress tensor of a medium is derived by the partial derivatives of elastic energy with respect to deformation tensor. It can be defined as;

$$\sigma_{ij} = \frac{\partial U}{\partial \epsilon_{ij}} \quad (5.3)$$

The stored elastic energy (U) in a medium is defined by the quadratic function of strain components of elastic tensor in the deformation stage of a medium (Babuška & Cara, 1991; Landau & Lifshitz, 1964). To draw the relation of elastic energy and strain tensors, Einstein summation are considered for repeated indices (lower).Thus,

$$U = C_{ijkl}\epsilon_{ij}\frac{\epsilon_{kl}}{2} \quad (5.4)$$

In the case of symmetricity of stress and strain tensor and using eqns.5.2 and 5.4, the coefficients of C_{ijkl} (stiffness tensor) decreases to 36 (in the ideal case, the coefficients of stiffness tensor are 81(3^4 =81)). Further, thermodynamics conditions (Nye, 1972) are applied on the solid elastic body that reduced elastic parameters to 21(Aki & Richards, 1980; Lay & Wallace, 1995). Therefore, on the basis of general law of elasticity, stiffness tensor can be defined as

$$C_{ijkl} = \begin{pmatrix} C_{1111} & C_{1122} & C_{1133} & C_{1123} & C_{1113} & C_{1112} \\ C_{2211} & C_{2222} & C_{2233} & C_{2223} & C_{2213} & C_{2212} \\ C_{3311} & C_{3322} & C_{3333} & C_{3323} & C_{3313} & C_{3312} \\ C_{2311} & C_{2322} & C_{2333} & C_{2323} & C_{2313} & C_{2312} \\ C_{1311} & C_{1322} & C_{1333} & C_{1323} & C_{1313} & C_{1312} \\ C_{1211} & C_{1222} & C_{1233} & C_{1223} & C_{1213} & C_{1212} \end{pmatrix} =$$

$$\begin{pmatrix} C_{11} & C_{12} & C_{13} & C_{14} & C_{15} & C_{16} \\ C_{21} & C_{22} & C_{23} & C_{24} & C_{25} & C_{26} \\ C_{31} & C_{32} & C_{33} & C_{34} & C_{35} & C_{36} \\ C_{41} & C_{42} & C_{43} & C_{44} & C_{45} & C_{46} \\ C_{51} & C_{52} & C_{53} & C_{54} & C_{55} & C_{56} \\ C_{61} & C_{62} & C_{63} & C_{64} & C_{65} & C_{66} \end{pmatrix}$$

For an anisotropic body, a number of 21 elastic coefficients are essential to define its elastic behaviour. The number of elastic coefficients varies according to the type of symmetry. The description of a number of elastic parameters with respect to different symmetric geometries is given below in Table 5.1.

Table 5-1 Details of numbers of elastic parameters for different symmetry geometries.

Sl.no	Type of symmetric system	Number of elastic parameters
1	Triclinic	21
2	Monoclinic	13
3	Orthorhombic	9
4	Tetragonal	6
5	Trigonal I	7
6	Trigonal II	6
7	Hexagonal	5
8	Cubic	3
9	Isotropic Solid	2

5.2.1 HEXAGONAL SYMMETRY

The elastic behaviour of typical rock forming minerals can be approximated by hexagonal symmetry (Montagner & Anderson, 1989). This kind of symmetry is also reported to be suitable for the elastic property of the medium containing aligned cracks and upper crust is one such medium (Crampin, 1978; Hudson, 1981; Kaneshima, 1991). Therefore, the crust should implicitly have seismic anisotropy of hexagonal symmetry. The hexagonal symmetry is mainly defined by two components: a single axis of rotation symmetry and a single plane of isotropy. This symmetric system can be originated due to the layered arrangement of materials having different elastic properties and alignment of minerals grains in crustal rocks. It is defined by five elastic parameters of the elastic media. If X3 is considered as the axis of symmetry, then the stiffness tensor of the horizontal symmetric system is defined as:

$$C_{\text{Horizontal}} = \begin{pmatrix} C_{11} & C_{12}-2C_{66} & C_{13} & 0 & 0 & 0 \\ C_{11}-2C_{66} & C_{11} & C_{13} & 0 & 0 & 0 \\ C_{13} & C_{13} & C_{33} & 0 & 0 & 0 \\ 0 & 0 & 0 & C_{55} & 0 & 0 \\ 0 & 0 & 0 & 0 & C_{55} & 0 \\ 0 & 0 & 0 & 0 & 0 & C_{66} \end{pmatrix}$$

Thus, for the parameterization of hexagonal symmetry in an anisotropic media, five elastic parameters are used to define the seismic velocities (*P*- and *S*-wave) as a function of propagation direction. Out of five parameters, two are orthogonal angles defines the orientation of symmetric axis, other two parameters are the percentage of anisotropies and one parameter illustrates the ellipticity of variation seismic velocities considered as constant.

5.3 CAUSES OF SEISMIC ANISOTROPY IN THE CRUST

5.3.1 EXTENSIVE-DILATANCY ANISOTROPY

Extensive-dilatancy anisotropy (EDA) is a phenomenon that arises due to the distribution of stress-aligned micro-cracks and joints in an anisotropic medium (Crampin et al., 1984). This type of dilatancy is the outcome of the growth of

cracks in a rock mass at low-stress levels (Atkinson, 1979, 1984). The arrangement of micro cracks pervaded in crustal rocks, allow the transmitted shear wave to split into fast and slow S-wavespropagates through the medium and perpendicular alignment of the cracks with the maximum stress direction makes it even more pronounced (Fig. 5.3).

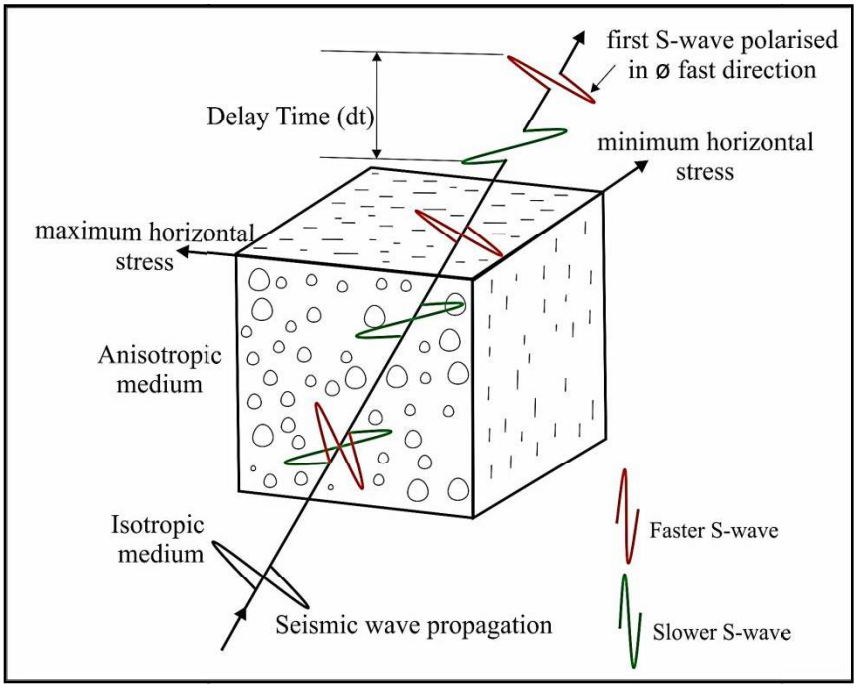

Figure 5.3 Illustration of extensive-dilatancy anisotropy with the distribution of stress-aligned fluid-saturated vertical cracks.

This is one of the phenomena of shear wave splitting in the upper crust (Crampin et al., 1984; Crampin & Lovell, 1991) and is a type of stress induced anisotropy. Such kind of anisotropy aligns fast axis (Φ) of the shear wave in a direction parallel to the maximum stress direction (Fig. 5.4). Crustal anisotropy resulting from such aligned cracks can be used not only to determine the state of stress in the crust but also the variations in the preferred orientation of cracks which may be an indication of a rotation c

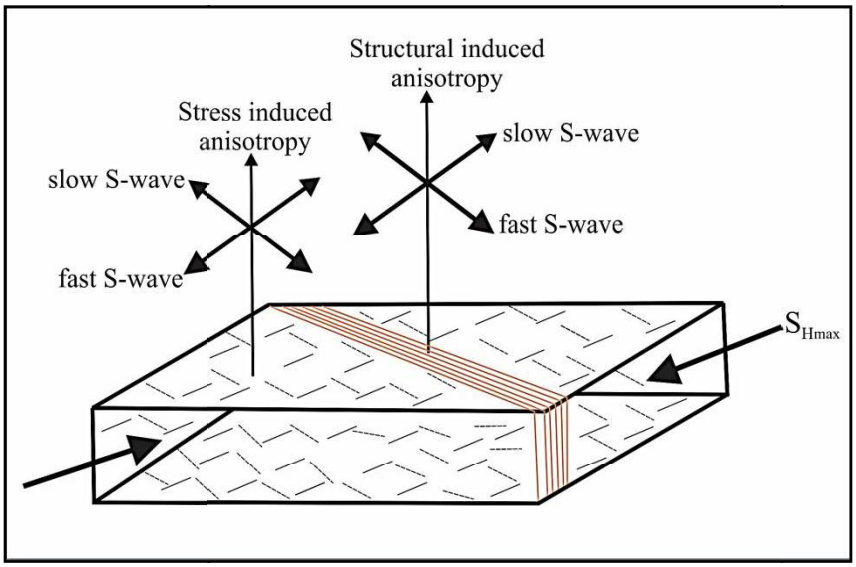

Figure 5.4 Illustration of two types of anisotropy in the crust; stress induced anisotropy adjacent to fault zone where fast shear (S)-wave polarized with fast direction parallel to maximum stress direction ($S_H$max) and structural induced anisotropy within fault zone where fast shear (S)-wave polarised parallel to fault fabric (modified after Bones & Zoback, 2006).

5.3.2 FRACTURING OF ROCK IN FAULT ZONES

This anisotropy is associated with alignment of macroscopic features such as fault zones, fabrics and fracture zones, and is a type of structure induced anisotropy. Minerals may get aligned due to shearing along fault zones resulting in fault-parallel Φ measurements for waves that traverse the fault-zone (Fig.5.4).

5.3.3 MINERAL ALIGNMENT INTRINSIC IN THE ROCK

Anisotropy from mineral alignment occurs when the crystals of a crystalline solid show different orientation on the passage of seismic waves over its specific volume and the minerals of crystals align to specific stress field and show preferred orientation in a particular plane (Crampin, 1984). In the presence of EDA cracks, the anisotropy due to the foliations has to be higher than that of the cracks to be detected. It is mainly observed in the upper mantle

of split shear wave. The mechanism of anisotropy resulted from the systematic orientation of minerals grains is referred as LPO.

5.3.4 LITHOLOGY ANISOTROPY

When the materials of a sedimentary column are deposited, the individual grains of sediments are distributed over a specific range and in the course; the particles get elongated or flattened. The shapes of sediments are uniformly aligned due to fluid flow or gravity during their deposition. Shale and clay are the examples of lithology anisotropy and observed to have a specific orientation of their mineral grains (Brodov et al., 1984; Robertson & Carrigan, 1983).

5.4 SEISMIC ANISOTROPY AND Ps SPLITTING

5.4.1 DATA USED FOR Ps SPLITTING

In this study, P-to-S converted phases (or *Ps* phase) of RFs originated at the Moho discontinuity is used for investigating crustal anisotropy beneath 13 stations in the Satluj valley (Fig. 5.5). The *Ps* phases of teleseismic earthquakes are usually contaminated with source effects and path effects and in most cases, it is difficult to recognize. This phase can be best isolated from source and path effects by computation of RFs (as described in Chapter 2).The deconvolution process used for computation of RFs removes the source and path effects and *Ps* phase becomes much clearer. The R and T components of RFs are utilized for analyzing *Ps* wave splitting to investigate crustal anisotropy.The *Ps* phase are selected from RFs of teleseismic earthquakes with $M_b \geq 5.5$ and Δ: 30^o-90^o based on the followingcriteria:(i) clear *Ps* phases both of RRF and TRF; (ii) analogous waveforms of the two components (iii) an elliptic particle wave motion before correction for anisotropy, (iv) a measurable time delay between slower and faster wave to rule out the appearance of energy in TRF. The significant energy in TRF may be due to the presence of inhomogeneities, such as dipping isotropic layers and/or scattering in the earth (Savage, 1998).

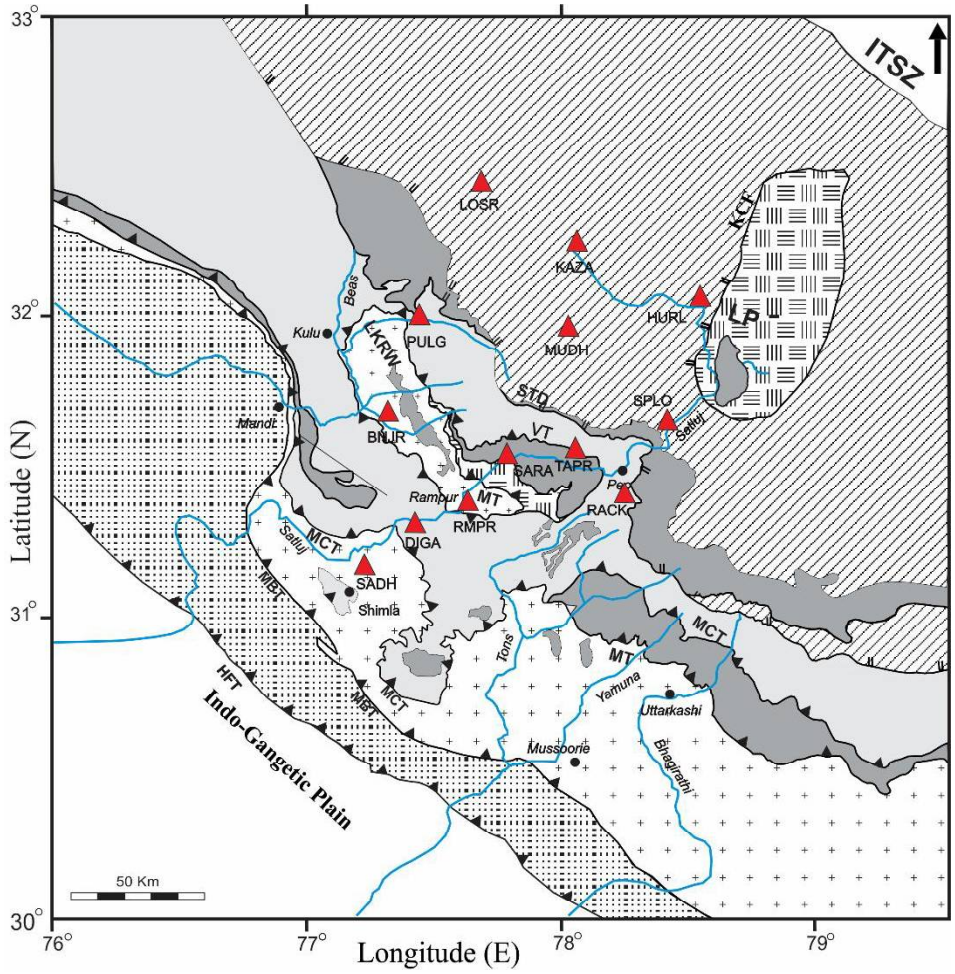

Figure 5.5 Locations of BBS stations used in the *Ps* splitting study shown by red triangles.

Following above-mentioned data selection criteria, a total of 137 numbers of *Ps* phases have been selected out of 124 teleseismic earthquakes recorded by at 13 BBS of LSAT and USAT networks (Fig. 5.5) and distribution of the selected earthquakes are shown in Figure 5.6. Total 4 BBS stations of LSAT network viz. SADH, DIGA, RMPR, TAPR and 9 BBS stations of USAT network viz. BNJR, SARA, RACK, PULG, MUDH, SPLO, LOSR, KAZA, and HURL have been used for this analysis. The rest of the stations are not used due to the complicated nature of *Ps* phases in the TRF.

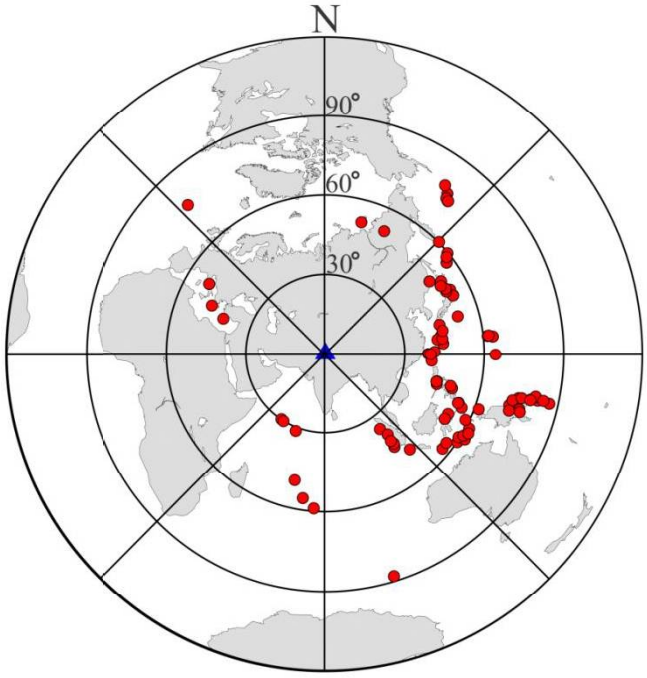

Figure 5.6 Spatial distribution of teleseismic earthquakes (red dot) used for Ps splitting study where blue triangle at the center shows network center.

5.4.2 SHEAR WAVE SPLITTING METHOD

A number of methods have been developed by different researchers for the estimation of shear wave splitting parameters, Φ and δt to characterize seismic anisotropy (Bowman & Ando, 1987; Silver & Chan, 1991; Zhang & Schwartz, 1994; Levin et al., 1999; Hao et al., 2008; Savage et al., 2010; Wuestefeld et al., 2010; Zaccarelli et al., 2012). Out of which of transverse component minimization method (Silver & Chan, 1988, 1991) and maximization of the cross-correlation method (Bowman & Ando, 1987; Levin et al., 1999) are most widely used. In the present study, cross-correlation method (Bowman & Ando, 1987) has been used to study shear wave splitting phenomena using *Ps* phases of RFs to investigate crustal anisotropy.

5.4.3 CROSS-CORRELATION METHOD

The cross-correlation method is based on the assumption that R and T components of the shear wave have the same shape but polarized in orthogonal directions with different velocities. It estimates the degree of

similarity between two different waveforms as a function of delay time relative to one another. The method involves finding a set of splitting parameters (Φ, δt) that maximize the correlation between the two orthogonal horizontal components. The grid search is applied over different values of Φ and δt in the domain of splitting parameters to obtained maximum cross-correlation coefficient. In the present study, a search was made for Φ from 0°-180° with an increment of 1° and for δt from 0.1 to 0.8 s to find a pair of Φ, δt that produce largest cross correlation value and the smallest root-mean-square misfit to the individual measurements.

The RFs are computed adopting methodology described in Chapter 2 with *Gw* 2.0. The *Ps* phase splitting analysis using the cross-correlation method is described considering RRFs and TRFs of a teleseismic earthquake recorded at KAZA station (Fig. 5.7).

The *Ps* phase is observed at 7.0 s in both the RRF and TRFs. The energy of *Ps* phase in the TRF is comparable with the RRF indicating the presence of anisotropy.

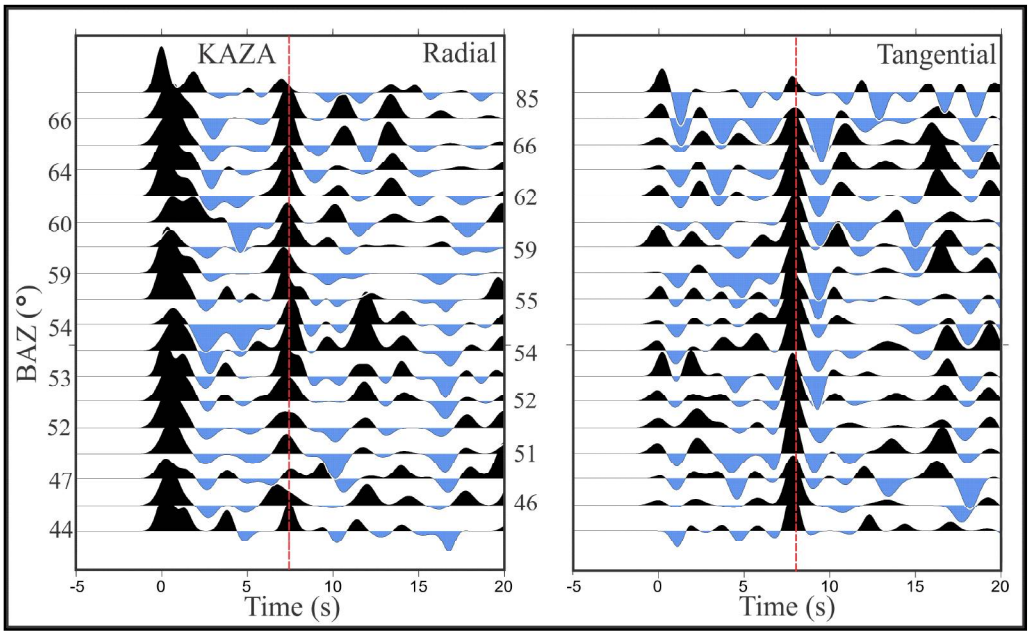

Figure 5.7 Example of radial and tangential components of RFs at KAZA station. A strong positive arrival is observed at ~7.0 s (marked by dotted red line) at radial and tangential components within a BAZ range 44° - 85°.

To describe the cross-correlation method, an example of RRF and TRF of KAZA station is shown in Figure 5.8. Initially, a window around the *Ps* phase is marked by A and F in both the radial and tangential components, (Fig.8*a*). The particle motion is obtained for selected window and after that, the cross correlation method has been applied to the selected window for

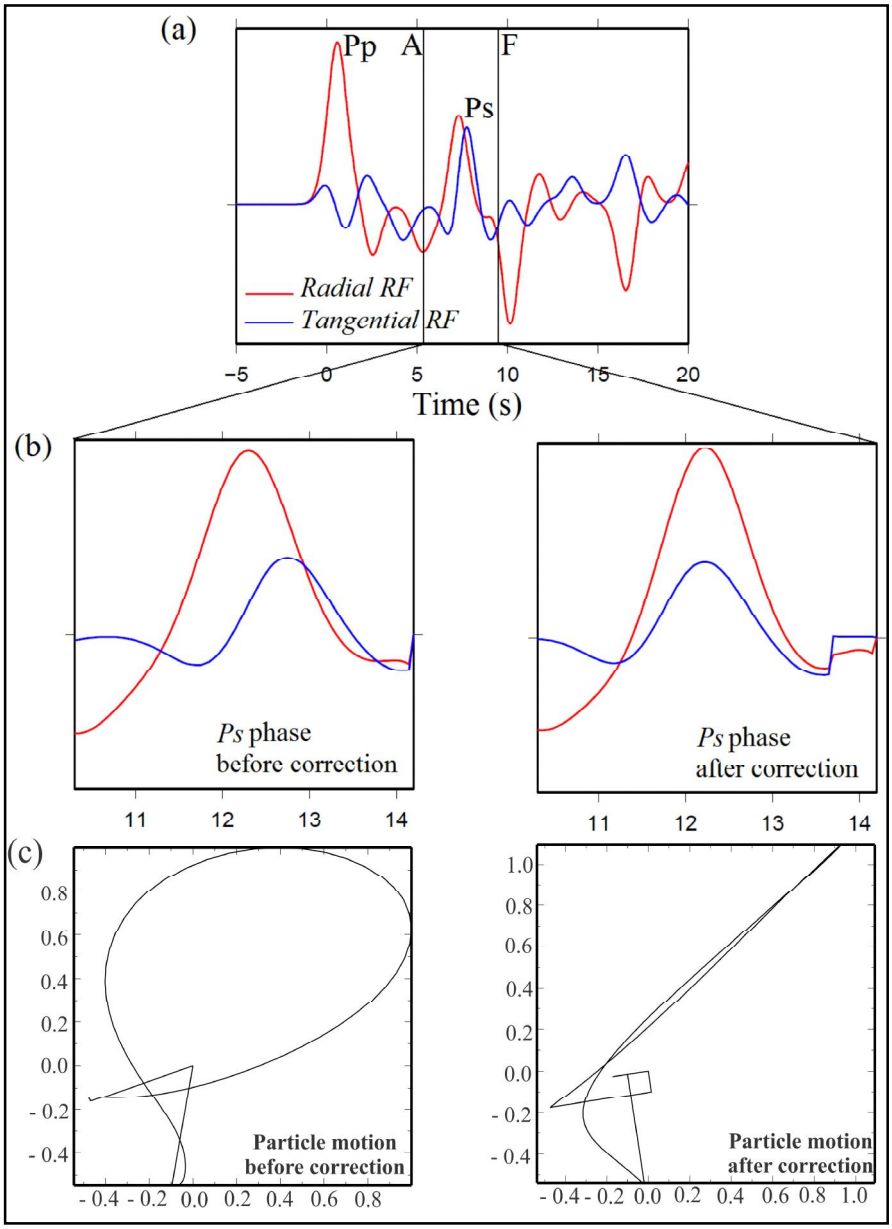

Figure 5.8 Example of Ps splitting of a teleseismic earthquake recorded at KAZA station using cross-correlation method. (a) Radial and tangential components of RF with Ps phase window marked by A and F, (b) Ps phase window before and after the correction for the anisotropy, and (c) the corresponding particle motion. The splitting parameters are, Φ: -30° and δt: 0.5 s.

correction of anisotropy. The particle motion obtained before and after the correction is shown in the middle panel (Fig. 5.8*b*) and the corresponding particle motions are shown in bottom panel (Fig. 5.8*c*). The elliptical particle motion suggests the presence of anisotropy while linear particle motion is observed after correction for anisotropy.

The result shows Φ: -30° and δt: 0.5 s with 15.6 as cross correlation value. The same analysis procedure has been adopted for splitting analysis of all *Ps* phases selected for seismic anisotropy study in the region.

5.4.4 Ps SPLITTING RESULTS

A total of 137 splitting parameters have been analyzed from 124 teleseismic earthquakes to compute shear wave splitting parameters for characterizing crustal anisotropy beneath 13 BBS stations. The *Ps* phase is originated at crust-mantle boundary below a recording station and vertically reaches the recording station bearing the anisotropic characteristics of the entire crust beneath the recording site. The individual values of splitting parameters (Φ, δt) are represented in Figure 5.10 and listed in Table 5.2. The FPDs are represented by the orientation of the black bars whereas the length of the bar indicatesdelay times between the fast and slow waves. Thus, the length of the bar is proportional to delay time and hence represents strength of anisotropy. The splitting parameters show variations at single stations and between different stations, yet a dominant NW-SE orientation of FPDs emerged among the measurements. The example of *Ps* phases both in radial and tangential components of RFs observed at few representative stations (BNJR, RMPR, SARA, TAPR, PULG and SPLO) located at different tectonic units i.e., LHS, LHCS, HHCS, and TH are shown in Figure 5.9*a*, *b*, *c*, *d*, *e* and *f*, respectively. The splitting parameters at individual stations are discussed below.

At SADH stations, very few *Ps* phases are obtained that pass the data selection criteria. The majority of data are discarded due to significant noise in the TRFs that masks the *Ps* phases. Only 4 *Ps* phases have been selected from

teleseismic waveform data arriving mostly from SE BAZ (Table 5.2, Fig. 5.10). Out of four parameters, FPDs of two events are oriented along NW-SE and other two follows NE-SW orientation with considerable delay time within the range 0.15 to 0.45 s. Due to less number of data, it is difficult to ascertain the reliable pattern of anisotropy direction at this station. However, the average pattern of FPD shows NW-SE orientation.

Table 5-2 List of teleseismic earthquakes used for Ps splitting analysis with their corresponding splitting parameters (Φ, δt) at each station.

Sl.No.	Event ID (YYYY-JJJ-HH:MM:SS.SS)	Origin Time (HH:MM:SS.SS)	Long. (°E)	Lat. (°N)	Depth (km)	Mag (M_b)	BAZ (deg.)	Station Code	FPD (Φ)	Delay Time (δt) (s)
1	2008-158-03:42:50.64	03:42:50.64	156.14	-7.43	75	5.1	102.61	RACK	-68	0.50
2	2008-164-11:00:08.49	11:00:08.49	144.95	12.76	35	5.4	90.69	SARA	-20	0.45
3	2008-165-23:43:45.36	23:43:45.36	140.88	39.03	7	6.9	62.97	SARA	-36	0.50
4	2008-174-23:56:30.03	23:56:30.03	141.27	67.70	18	6.1	26.21	LOSR	-62	0.35
5	2008-177-01:52:36.04	01:52:36.04	97.15	1.32	19	5.5	144.74	HURL	58	0.40
							145.29	SPLO	-40	0.50
6	2008-177-15:41:28.00	15:41:28.00	151.69	-5.27	50	5.7	102.90	HURL	-84	0.20
							102.90	PULG	-8	0.45
7	2008-181-17:02:18.88	17:02:18.88	-169.92	51.92	25	5.4	35.81	SPLO	-66	0.35
8	2008-181-20:53:04.89	20:53:04.89	137.44	45.16	326	6.0	56.05	KAZA	68	0.60
							55.44	SARA	-56	0.25

9	2008-186-04:55:05.31	04:55:05.31	133.95	75.40	10	5.0	15.51	SARA	-56	0.50
10	2008-188-01:00:08.83	01:00:08.83	151.04	45.35	22	5.7	53.65	KAZA	74	0.35
							53.34	SARA	-14	0.45
11	2008-188-09:08:21.29	09:08:21.29	150.96	45.39	17	5.7	53.63	KAZA	-56	0.35
							53.32	SARA	-66	0.40
12	2008-189-22:43:50.84	22:43:50.84	-177.06	51.94	67	5.3	38.30	SARA	-74	0.45
13	2008-190-07:42:10.73	07:42:10.73	128.33	27.53	43	6.0	81.72	SPLO	-74	0.35
14	2008-193-09:58:49.93	09:58:49.93	147.82	-2.94	23	5.7	103.17	HURL	-56	0.35
15	2008-193-21:35:06.45	21:35:06.45	121.13	21.02	6	5.5	94.95	HURL	-30	0.80
16	2008-201-02:39:28.70	02:39:28.70	142.21	37.55	22	7.0	64.94	KAZA	86	0.55
17	2008-202-08:2142.17	08:2142.17	62.09	4.87	10	5.3	212.68	SARA	-52	0.50
18	2008-205-15:26:19.95	15:26:19.95	141.46	39.80	108	6.8	61.88	SARA	-8	0.45
19	2008-206-01:43:16.14	01:43:16.14	157.58	50.97	27	6.2	45.97	LOSR	-70	0.40
20	2008-209-19:30:50.08	19:30:50.08	126.49	-7.36	314	5.2	121.35	SPLO	-60	0.35
21	2008-210-07:10:04.58	07:10:04.58	99.79	-1.07	84	5.3	143.46	SARA	-24	0.35
22	2008-214-10:35:24.26	10:35:24.26	120.75	13.52	135	5.6	104.97	PULG	-80	0.50
23	2008-217-03:26:50.44	03:26:50.44	120.31	-8.20	39	5.1	127.11	SPLO	-44	0.50
24	2008-218-01:00:46.60	01:00:46.60	126.48	26.98	16	5.2	83.23	SPLO	-26	0.50
25	2008-222-11:54:19.71	11:54:19.71	128.52	26.49	24	5.2	83.08	SARA	-24	0.50
26	2008-222-15:18:16.90	15:18:16.9	-178.44	51.50	58	5.5	39.02	LOSR	72	0.25

27	2008-229-08:26:23.99	08:26:23.99	61.30	5.52	10	5.1	214.66	SPLO	-52	0.50
28	2008-238-02:43:06.36	02:43:06.36	125.25	10.31	27	5.8	105.16	SPLO	-12	0.35
29	2008-243-06:54:07.61	06:54:07.61	147.26	-6.15	75	6.4	106.21	PULG	-80	0.50
30	2008-251-02:05:00.92	02:05:00.92	69.49	-23.71	10	5.4	189.48	SARA	-44	0.50
31	2008-255-00:00:02.70	00:00:02.70	127.36	1.89	96	6.6	112.28	KAZA	-66	0.70
32	2008-259-05:41:46.09	05:41:46.09	-178.35	51.40	31	5.2	39.20	SARA	-40	0.35
33	2008-260-01:12:52.75	01:12:52.75	127.93	-2.45	35	5.3	115.96	SARA	-52	0.50
34	2008-260-11:15:41.27	11:15:41.27	126.84	-8.78	35	5.7	122.02	KAZA	-58	0.60
35	2008-266-07:31:59.17	07:31:59.17	140.45	41.58	149	5.6	60.31	KAZA	58	0.60
							59.80	SARA	-8	0.40
36	2008-271-03:04:51.71	03:04:51.71	120.58	13.47	10	5.7	104.88	RACK	-14	0.50
37	2008-271-03:09:04.82	03:09:04.82	120.55	13.48	11	5.9	104.89	RACK	-8	0.50
38	2008-275-09:38:12.32	09:38:12.32	138.78	30.17	413	5.7	74.93	LOSR	84	0.30
39	2008-275-18:06:49.81	18:06:49.81	120.57	13.47	10	5.2	104.89	SARA	-48	0.50
40	2008-292-00:54:39.65	00:54:39.65	147.27	-6.95	77	5.7	106.88	PULG	-82	0.50
41	2008-294-04:54:19.24	04:54:19.24	120.68	0.11	96	5.9	119.30	PULG	-34	0.35
42	2008-296-00:39:28.40	00:39:28.40	130.04	28.85	38	5.2	79.27	SARA	-2	0.50
43	2008-297-10:04:35.04	10:04:35.04	145.57	-2.64	10	6.3	104.24	KAZA	-72	0.50
44	2008-300-10:27:37.49	10:27:37.49	100.75	-3.63	35	5.1	144.19	SARA	-20	0.50
45	2008-304-	01:55:14.19	153.21	46.43	32	5.5	51.97	KAZA	-28	0.65

	01:55:14.19									
							51.69	SARA	-64	0.35
46	2008-306-04:08:59.28	04:08:59.28	148.87	-3.42	10	5.7	102.96	LOSR	-88	0.40
47	2008-307-13:48:42.82	13:48:42.82	-174.37	51.55	36	6.1	37.56	LOSR	-64	0.35
48	2008-316-12:18:12.77	12:18:12.77	66.7	1.59	10	5.1	201.97	SARA	-58	0.45
49	2008-322-06:00:58.91	06:00:58.91	128.80	-5.66	306	5.6	117.94	HURL	-38	0.50
50	2008-324-00:54:45.89	00:54:45.89	143.6	-5.03	115	5.0	107.71	SARA	-58	0.50
51	2008-324-15:20:58.05	15:20:58.05	-27.45	47.37	10	5.0	317.90	RACK	-40	0.50
52	2008-333-08:50:48.19	08:50:48.19	101.75	-4.74	27	5.8	143.73	RACK	-42	0.50
53	2008-335-00:38:54.07	00:38:54.07	146.99	18.02	14	5.6	84.50	PULG	-82	0.50
54	2008-335-12:04:54.96	12:04:54.96	145.34	19.19	207	5.0	84.07	RACK	-10	0.50
55	2008-337-03:16:53.3	03:16:53.30	121.60	23.28	29	5.1	90.87	SARA	-6	0.45
56	2008-337-12:31:43.88	12:31:43.88	145.75	19.11	137	5.9	83.96	RACK	-2	0.35
57	2008-338-23:16:54.87	23:16:54.87	142.88	38.59	14	5.8	63.51	KAZA	64	0.55
							63.51	PULG	-6	0.40
58	2008-341-10:55:26.35	10:55:26.35	124.75	-7.39	398	6.4	122.52	KAZA	-42	0.65
59	2008-343-18:39:09.31	18:39:09.31	106.82	-53.00	10	6.3	163.15	RACK	6	0.40
60	2008-355-10:29:23.1	10:29:23.10	142.43	36.54	19	6.3	66.10	KAZA	-30	0.45
61	2008-356-09:16:44.74	09:16:44.74	142.32	36.54	13	5.9	66.13	PULG	-42	0.50
62	2009-004-05:44:04.42	05:44:04.42	133.19	-0.67	31	5.7	110.43	KAZA	-80	0.65
63	2009-015-	17:49:39.07	155.15	46.86	36	7.4	51.06	KAZA	-30	0.50

	17:49:39.07									
64	2009-028-07:53:38.19	07:53:38.19	124.16	-8.94	65	5.7	124.25	HURL	-80	0.50
65	2009-042-17:34:50.80	17:34:50.80	126.40	3.88	22	7.2	111.10	RACK	0	0.50
66	2009-042-17:44:04.62	17:44:04.62	126.64	3.88	29	5.5	110.91	HURL	-78	0.40
67	2009-047-23:16:38.5	23:16:38.50	20.78	37.13	15	5.4	293.42	RACK	-62	0.45
68	2009-059-00:35:56.7	00:35:56.70	142.10	42.61	105	5.5	58.70	KAZA	-20	0.40
							58.22	RACK	-20	0.40
69	2009-060-19:46:58.95	19:46:58.95	128.29	-7.15	35	5.1	119.80	RACK	-36	0.45
70	2009-075-17:42:03.58	17:42:03.58	126.70	3.60	18	5.7	111.14	HURL	-72	0.25
71	2009-083-23:28:28.05	23:28:28.05	151.82	-5.14	43	5.8	102.72	KAZA	-72	0.65
72	2009-085-06:14:22.14	06:14:22.14	73.30	-27.46	10	5.7	184.90	RACK	-62	0.45
73	2009-089-12:07:28.18	12:07:28.18	-178.26	51.54	31	5.7	38.93	PULG	-24	0.45
74	2009-091-03:54:58.77	03:54:58.77	144.10	-3.52	10	6.4	105.88	HURL	42	0.50
75	2009-091-06:29:40.39	06:29:40.39	101.91	-5.96	35	5.6	143.93	KAZA	-38	0.80
76	2009-097-17:47:37.00	17:47:37.00	13.46	42.28	15	5.5	300.66	KAZA	-44	0.40
							301.44	RACK	-42	0.50
77	2009-106-00:43:20.7	00:43:20.70	154.15	-6.48	10	5.8	102.54	BNJR	-10	0.35
78	2009-170-14:04:59.03	14:04:59.03	28.45	35.36	28	5.8	288.20	BNJR	-80	0.50
79	2009-174-14:19:17.76	14:19:17.76	153.70	-5.20	65	5.5	101.72	BNJR	-78	0.35
80	2009-174-14:19:22.35	14:19:22.35	153.78	-5.16	64	6.7	101.63	BNJR	-78	0.35
							101.63	MUDH	-40	0.30

81	2009-179-14:19:30.00	14:19:30.00	122.20	1.38	36	5.7	116.82	MUDH	-54	0.50
82	2009-187-22:35:05.02	22:35:05.02	128.03	24.87	10	5.7	86.00	PULG	2	0.50
83	2009-230-13:17:35.27	13:17:35.27	123.52	23.51	5	5.6	90.12	PULG	-2	0.50
84	2009-245-07:55:01.05	07:55:01.05	107.30	-7.78	46	7.0	139.05	PULG	-58	0.45
85	2009-246-13:26:18.24	13:26:18.24	130.02	31.14	165	6.2	76.75	MUDH	-16	0.45
86	2009-261-06:23:53.49	06:23:53.49	120.43	12.62	12	6.0	106.30	MUDH	-50	0.20
87	2009-282-22:49:54.09	22:49:54.09	157.96	-9.03	10	5.6	102.57	MUDH	-8	0.50
88	2009-285-03:15:47.28	:03:15:47.28	66.69	-17.10	10	6.2	193.06	BNJR	-42	0.50
89	2009-297-20:54:50.84	-20:54:50.84	118.79	-9.90	35	5.6	129.49	MUDH	-50	0.50
90	2009-309-09:32:56.56	09:32:56.56	120.74	23.73	18	5.6	91.32	BNJR	-10	0.25
91	2009-309-11:34:18.88	11:34:18.88	120.84	23.66	10	5.5	91.38	BNJR	-28	0.40
92	2009-315-13:48:19.24	13:48:19.24	125.53	9.36	23	5.7	106.13	BNJR	-58	0.50
93	2013-322-19:10:45.03	19:10:45.03	34.33	137.05	328	5.6	69.43	RMPR	-80	0.25
94	2013-326-17:20:58.34	17:20:58.34	5.42	92.82	15	5.5	147.16	DIGA	56	0.50
95	2013-335-06:29:57.80	06:29:57.80	2.04	96.83	20	6	143.68	TAPR	-52	0.35
96	2013-351-23:38:06.82	23:38:06.82	20.77	146.79	9	6.2	81.26	TAPR	-28	0.40
97	2013-357-06:57:29.11	06:57:29.11	35.69	142.14	8	5.6	66.42	RMPR	-14	0.45
98	2014-026-13:55:42.21	13:55:42.21	38.21	20.45	8	6.1	295.00	DIGA	-52	0.20
99	2014-034-22:36:37.09	22:36:37.09	-7.19	128.17	7	5.8	119.18	RMPR	-28	0.35

100	2014-055-23:26:55.07	23:26:55.07	4.13	62.88	4	5.6	209.38	TAPR	-66	0.50
101	2014-055-23:59:45.78	23:59:45.78	4.23	62.52	10	5.5	210.09	TAPR	-56	0.50
102	2014-093-09:30:24.93	09:30:24.93	-5.24	102.28	44	5.7	142.24	TAPR	-40	0.50
103	2014-094-11:40:32:00	11:40:32:00	-10.54	161.70	57	6	101.84	RMPR	-10	0.30
104	2014-094-20:08:06.97	20:08:06.97	37.28	23.87	107	5.6	293.12	RMPR	-70	0.50
105	2014-101-07:07:23.13	07:07:23.13	-6.59	155.05	60	7.1	102.00	RMPR	-40	0.45
106	2014-185-13:12:18.39	13:12:18.39	-7.01	155.85	42	5.6	101.92	TAPR	-58	0.45
107	2014-185-22:42:04.74	22:42:04.74	39.68	142.03	44	5.7	61.58	DIGA	-44	0.45
108	2014-195:08:00:00.09	08:00:00.09	5.68	126.57	44	6.3	52.72	SADH	-64	0.45
109	2014-210-22:04:43.5	22:04:43.50	35.38	-36.26	10	5.5	88.80	SADH	56	0.30
110	2014-233-02:11:31.04	02:11:31.04	-5.29	150.69	8	5.9	103.44	RMPR	-72	0.30
111	2014-253-05:16:53.21	05:16:53.21	-0.18	125.13	30	5.9	115.49	RMPR	-46	0.45
112	2014-263-18:27:13.71	18:27:13.71	-0.77	134.30	12	5.5	62.61	SADH	-74	0.45
113	2014-266-15:24:00.53	15:24:00.53	-5.40	151.74	57	5.5	102.95	RMPR	-56	0.45
114	2014-274-03:38:51.76	03:38:51.76	-6.07	149.53	42	6	78.10	SADH	78	0.15
115	2014-275-12:57:05.75	12:57:05.75	52.32	158.05	143	5.7	44.01	DIGA	-50	0.50
116	2014-280-10:22:30.75	10:22:30.75	64.53	-17.20	4	5.5	331.50	DIGA	-58	0.45
117	2014-284-02:35:47.48	02:35:47.48	41.03	143.17	22	6.1	59.84	DIGA	-52	0.40
							59.84	RMPR	-58	0.25

118	2014-319-02:31:41.72	02:31:41.72	1.89	126.52	45	7.1	112.44	RMPR	-34	0.50
119	2014-319-09:47:57.85	09:47:57.85	1.79	126.56	35	5.5	112.51	RMPR	-58	0.50
120	2014-322-04:47:16.63	04:47:16.63	1.87	126.48	30	5.8	112.50	RMPR	-40	0.40
121	2014-325-10:10:19.63	10:10:19.63	2.30	127.06	35	6.5	111.65	DIGA	-42	0.25
122	2014-330-14:33.43.64	14:33.43.64	1.96	126.58	39	6.8	112.34	RMPR	-40	0.45
							112.34	DIGA	-44	0.35
123	2015-012-20:25:14.17	20:25:14.17	-5.59	133.92	21	5.6	113.96	DIGA	52	0.35
124	2015-056-07:01:01.07	07:01:01.07	31.10	141.84	9	5.9	72.13	RMPR	-44	0.45

A similar pattern is also observed at DIGA station. Out of 9 events, 7 events show NW-SE FPDs and other two shows NE-SW FPDs. Total 15 splitting parameters have been computed in RMPR station located over the LKRW. At this station, the FPDs are consistently observed to be oriented along NW-SE direction. The FPD varies from -10° to -80° with the significant strength of anisotropy represented by delay time within the range of δt: 0.25 to 0.50 s. The BNJR station also shows the similar trend with FPD range -10° to -80°; δt: 0.26-0.50 s. A total number of 20 splitting parameters have been computed at SARA station that shows NW-SE trend with FPD ranging from -2° to -74° and delay time δt: 0.25 to 0.60 s. Total 12 splitting parameters computed at PULG station shows a wide range of FPD from -2° to -80° with considerable delay time δt: 0.35 to 0.50 s.

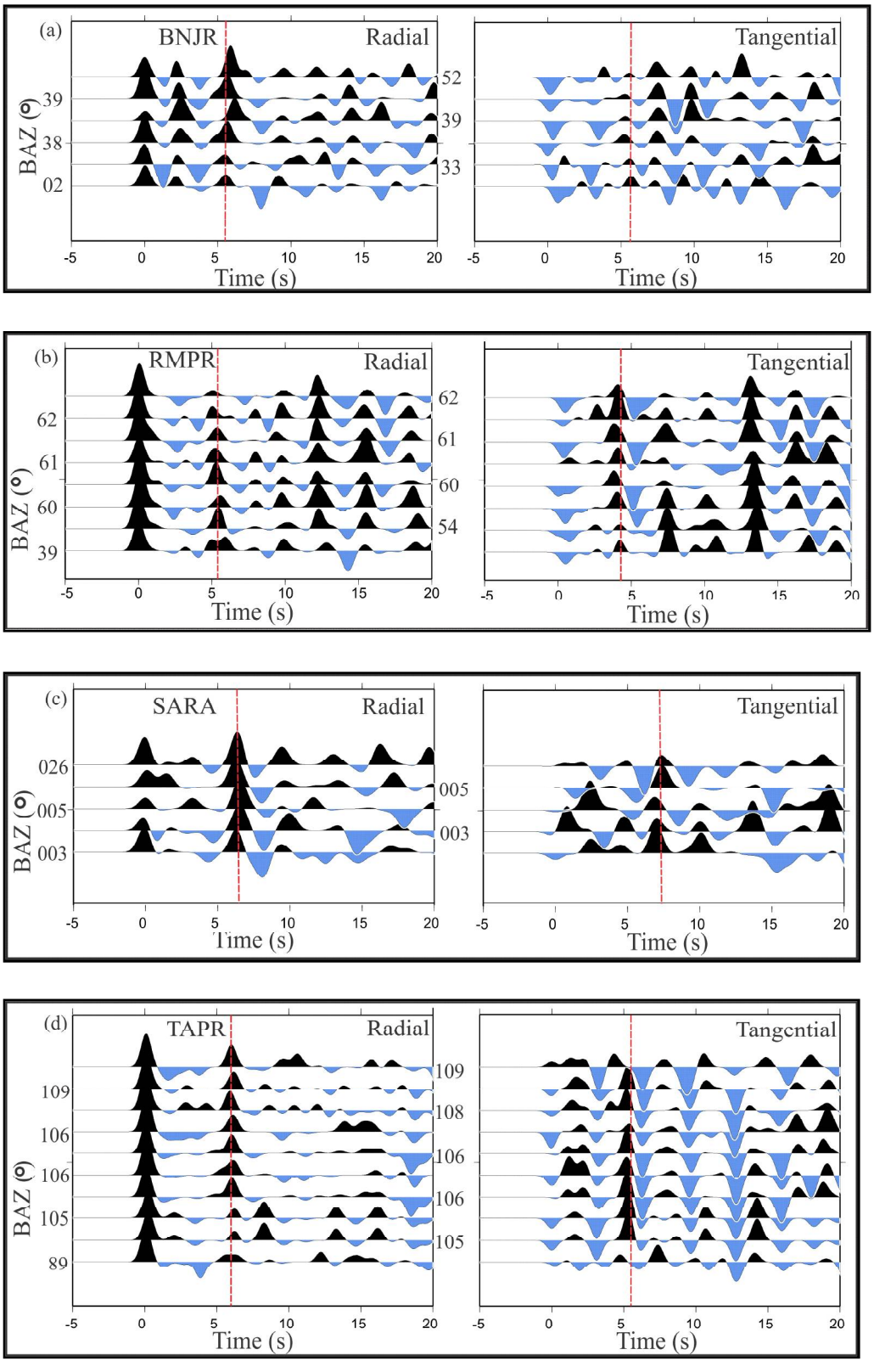
(a)
BNJR
Radial
Tangential
BAZ (°)
39
38
02
52
39
33
-5
0
5
10
15
20
Time (s)
(b)
RMPR
Radial
Tangential
BAZ (°)
62
61
60
39
62
61
60
54
Time (s)
(c)
SARA
Radial
Tangential
BAZ (°)
026
005
003
005
003
Time (s)
(d)
TAPR
Radial
Tangential
BAZ (°)
109
106
106
105
89
109
108
106
106
105
Time (s)

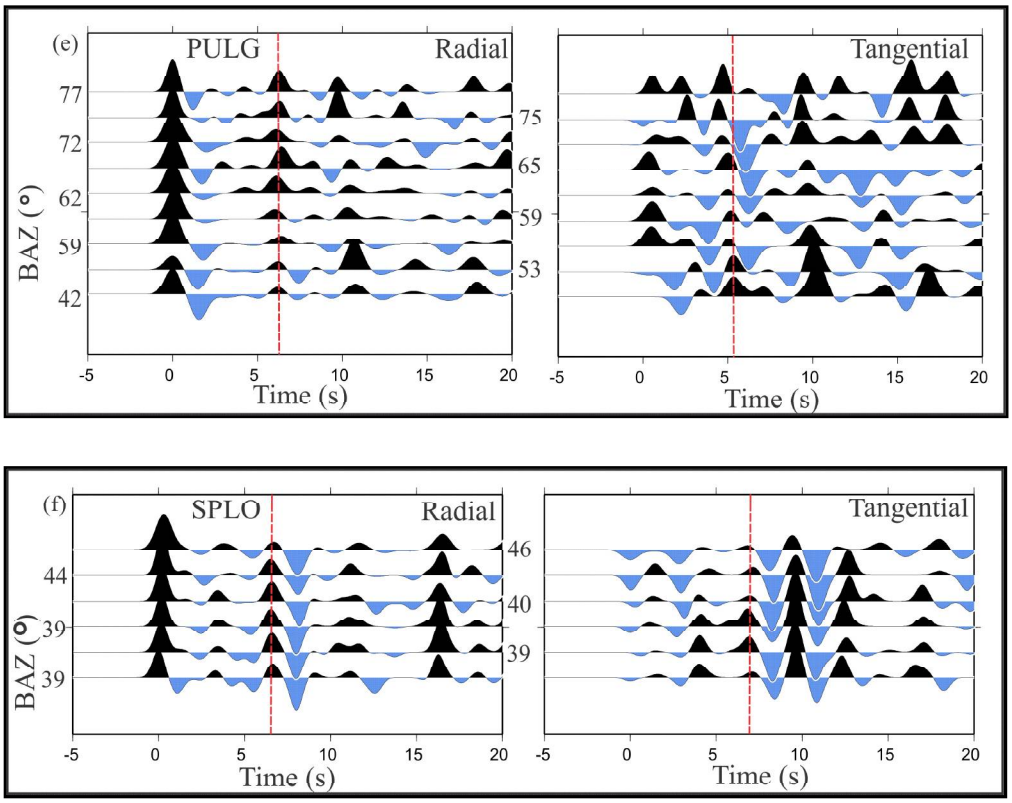

Figure 5.9 Example of radial and tangential components of RFs of6 stations located at different tectonic units (a) BNJR in LHS, (b) RMPR and (c) SARA in LHCS, (d) TAPR, (e) PULG, in HHCS and (f) SPLO in TH. The strong Ps is marked by dotted red line both in RRFs and TRFs with respective BAZ.

The TAPR and SPLO show similar FPD trend (FPD ranging from -12° to -74°). The majority of splitting parameters at RACK stations located close to the STD shows NNW-SSE trend. The LOSR is the northern most station where only 6 pairs of splitting parameters have been computed with large cross correlation parameter. The FPDs at LOSR follows roughly E-W trend. Total 6 best selected *Ps* phases have been analyzed at MUDH station and results show NW-SE oriented FPDs with delay time δt: 0.20 to 0.53 s. The FPD is widely distributed at KAZA station. Total 19 pairs of splitting parameters have been computed at this station, out of which 14 FPDs are oriented along NW-SE and only 5 events show NE orientation. The splitting parameters show complicated FPDs at KAZA station showing both NW and NE oriented FPDs and the delay time ranges from 0.35 to 0.80 s.

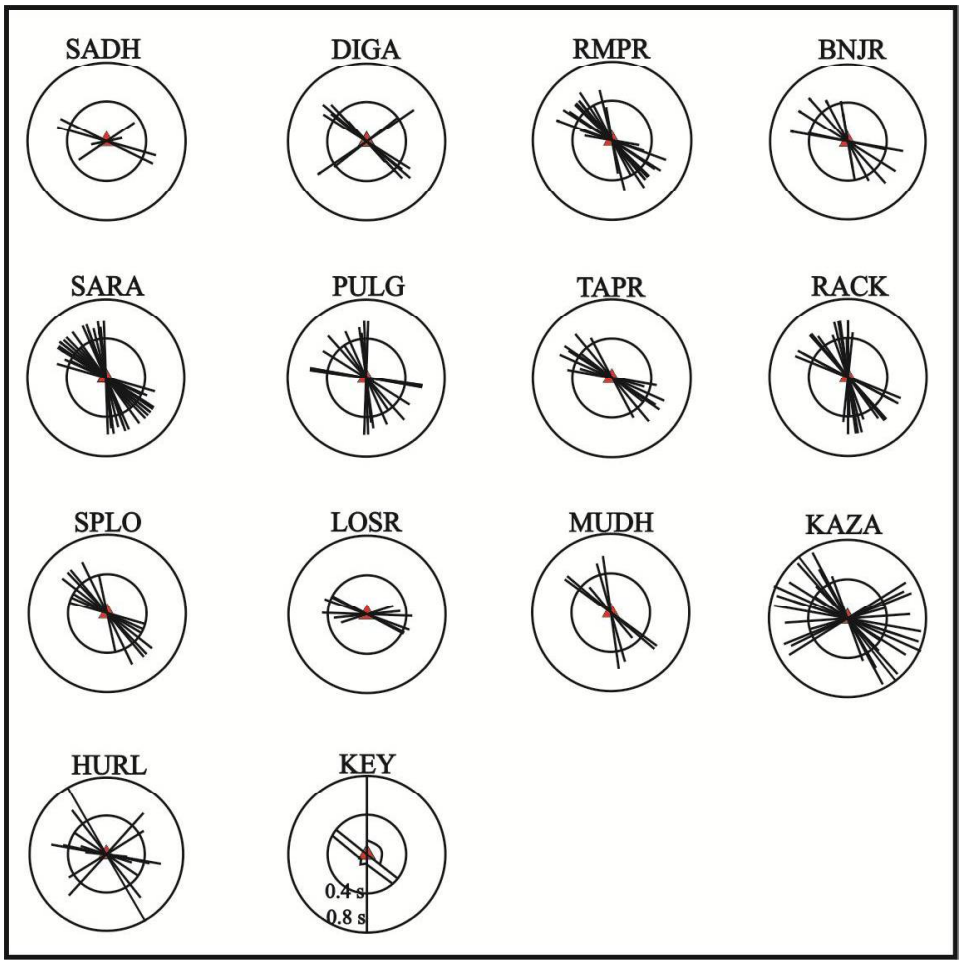

Figure 5.10 Results of individual splitting measurements (Φ, δt) at each of the 13 stations (red triangles) .The lower right panel shows a key to represent the plotting at individual stations. The delay time ranges from 0.15 to 0.80 s.

In order to portray the average trend of FPD and delay times at each station the splitting parameters at each station, are averaged. The average splitting parameters at individual stations are listed in Table 5.3 and the FPDs are shown in Figure 5.11.

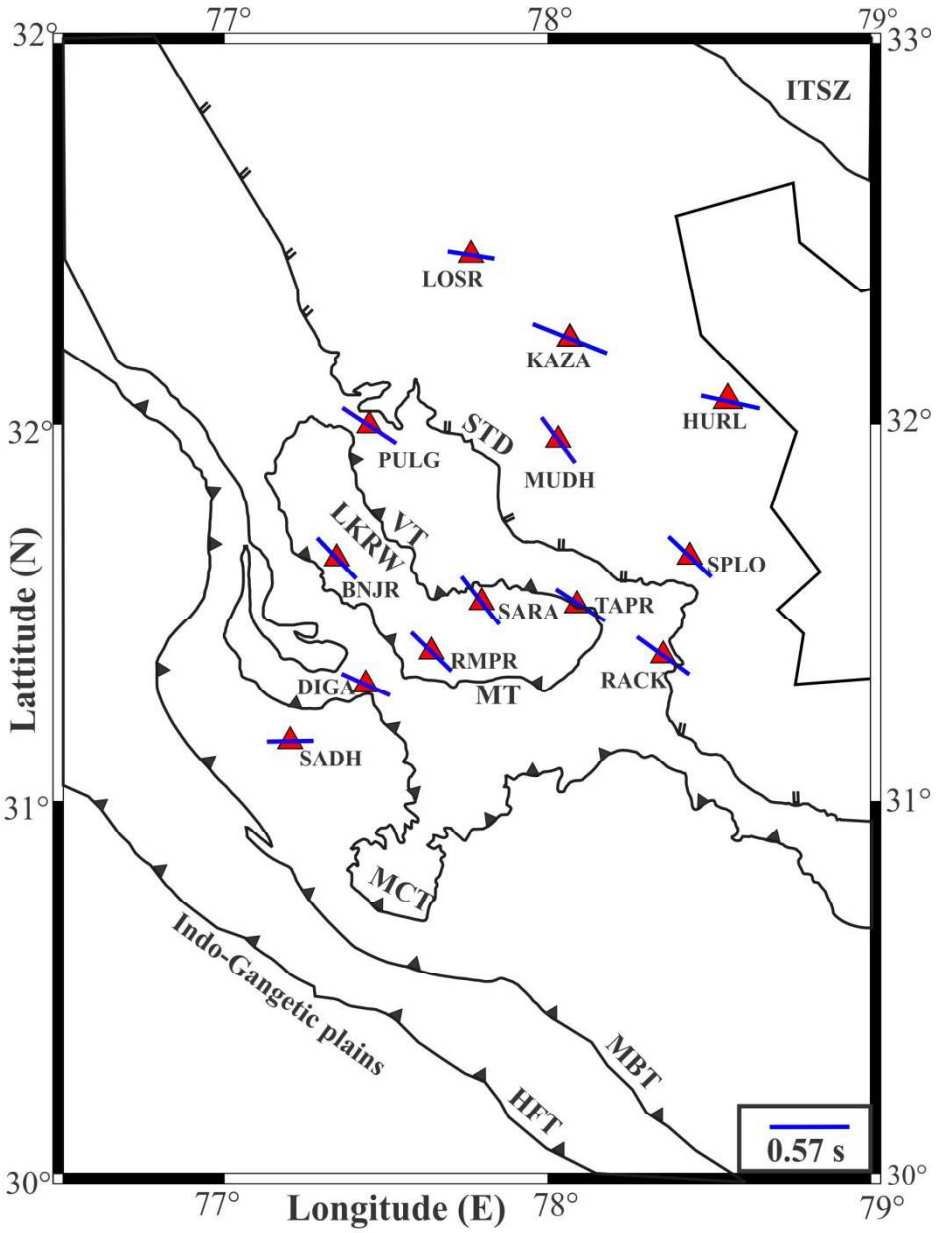

Figure 5.11 Distribution of average fast polarization direction (Φ) at each station (red triangles) estimated through *Ps* phase splitting. The lower right inset shows the scale of delay time (δt).

Table 5-3 List of average splitting parameters (Φ, δt) at each station.

Sl.no.	Station Code	Longitude (°E)	Latitude (°N)	Average FPD (degrees)	Average Delay Time (s)
1	SADH	77.203	31.159	89.00	0.34
2	DIGA	77.437	31.309	114.00	0.38
3	RMPR	77.640	31.396	134.00	0.40
4	BNJR	77.347	31.646	136.28	0.41
5	SARA	77.792	31.533	142.27	0.45
6	PULG	77.448	31.997	123.66	0.47
7	TAPR	78.091	31.521	123.25	0.43
8	RACK	78.358	31.386	125.71	0.46
9	SPLO	78.441	31.650	133.25	0.43
10	LOSR	77.763	32.446	98.666	0.34
11	MUDH	78.033	31.959	143.66	0.41
12	KAZA	78.069	32.227	111.47	0.57
13	HURL	78.552	32.061	102.44	0.43

Despite the complicated nature of individual FPD measurements at few stations, predominant FPD in the region are oriented along NW-SE. In most cases, the FPDs appear to follows surface geological features rather than the overall compressive stress pattern of NW Himalaya. It is evident from the results that seismic anisotropy is significantly strong in the crust. The inferences of the results are discussed in the discussion section.

5.5 ULTRASONIC MEASUREMENTS OF ROCK SAMPLES

5.5.1 SAMPLING LOCATION AND PREPARATION OF THE SAMPLES

Fresh rock samples of different lithology namely slates, gneisses, quartzites, and granites were collected from various locations along the Satluj valley. Three block samples of slates (Tethyan meta-sedimentary) were taken from

the Tethyan Himalaya near Pooh and another two block samples of slates were collected from the transition zone of the TH near Morang. Four samples of granitic gneisses were collected from a thick sequence of the HHCS near Kalpa and Karcham. Five block samples of granites were collected near Akpa from the HHCS. Four blocks of augen gneisses were taken from a thick sequence of the WGC, near Wangtu. Furthermore, five blocks of quartzites were collected from Rampur window near Rampur, Shimla. The locations of each sample are marked in Figure 5.12. The dimension of each block was approximately 75cm x 100cm x 100cm. Thus, total number of 23 samples was collected from the study area.

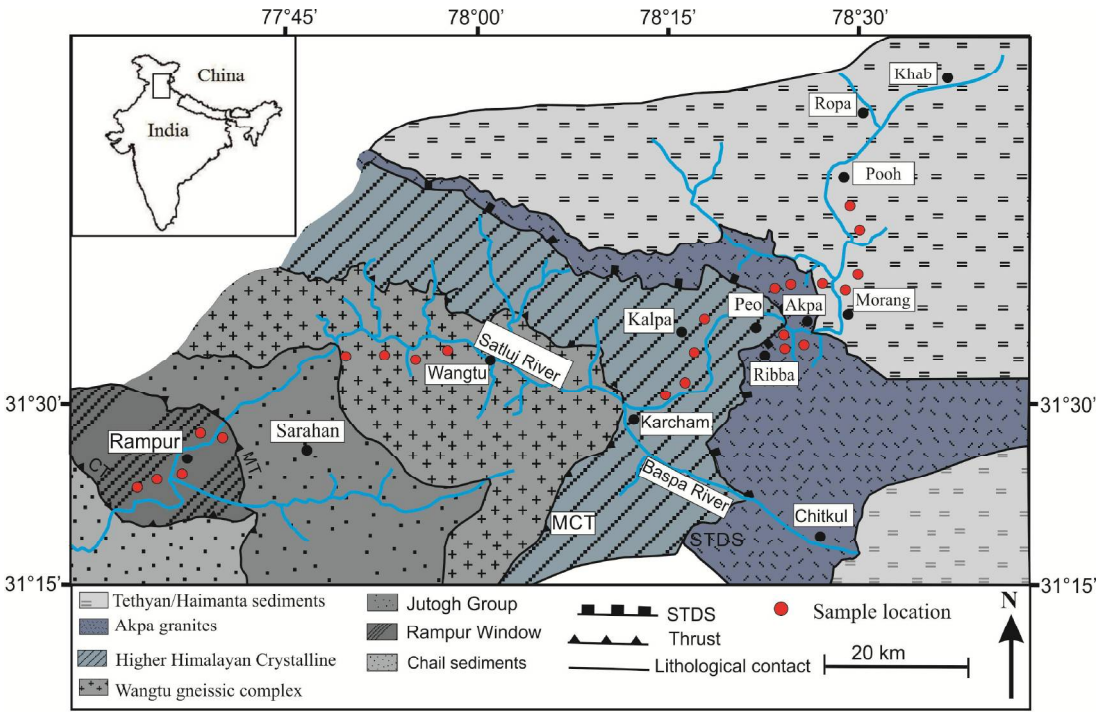

Figure 5.12 Locations of samples collected from Satluj valley (map is modified after Caddick et al., 2007).

All the collected samples are free from any micro structural discontinuity like cracks and joints. Each sample was drilled to obtain about four cylindrically shaped samples by cutting it into two orthogonal directions that are perpendicular and parallel to the foliation plane of rock specimen. Thus, total 92 cylindrical cores were drilled from 23 block samples. All

cylindrical cores were of 2.50 cm in diameter and 4.0-5.0 cm in length (Fig. 5.13).

The end surfaces of the cylindrical cores are smooth and parallel with in an accuracy of 0.50 mm so that they make good contact with ultrasonic transducers. It has been found that the unparalleled and undulating surfaces result into noisy and attenuated signals which may increase the possibility of error in measurements.

Figure 5.13 Photograph showing the cylindrical cores samples.

5.5.2 EXPERIMENTAL SETUP FOR ULTRASONIC MEASUREMENTS

The measurement of seismic velocities of core samples has been done using ULT-100-Ultrasonic velocity testing system (Fig. 5.14). It consists of a pulser generator unit, two transducers i.e. transmitter and receiver and a data acquisition with a processing unit.

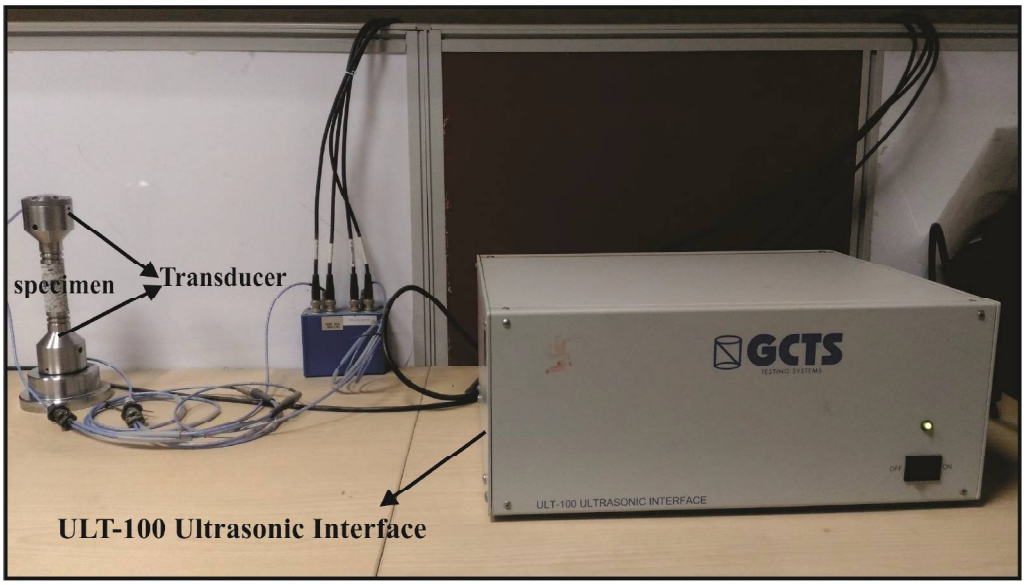

Figure 5.14 Ultrasonic velocity testing system comprises of high energy ultrasonic interface and transducers used in laboratory at room temperature and pressure conditions.

The pulser unit is a high energy unit which provides an electric signal to rock specimen which is then transformed into a seismic signal by using a piezoelectric transmitter transducer. The transmitted seismic signal travels through the cylindrical core and then, received by receiver transducer. Further, the receiver transducer converts the seismic signal into an electrical signal which is then received by receiving unit of pulser. The received electrical signal is then processed by data acquisition board and displayed on the screen of attached electronic device. The transducers usually have an operating pulse frequency between 200 kHz and 1000 kHz.

The piezoelectric crystal of transducer is protected by a metal face, thus there will be some delay in receiving signal. The delay of the reference signal can be determined by a test which involves placing top and bottom platens directly together; this test is referred as face-to-face delay time test. An acoustic couplant such as honey or machine oil is used to remove the irregularities of the specimen and passage of air between the testing specimen and test platens. The use of couplant increases the quality and transmits cleared seismic signal to the receiving end.

5.5.3 ULTRASONIC MEASUREMENTS

The measurement of seismic wave velocities (*P*-and *S*-wave) has been done using 'time of flight' ultrasonic pulse transmission (ULT) technique (Birch, 1960; Ramana & Rao, 1974; Rao & Lakshmi, 2003) at room P-T conditions. This technique determines the P-and S-wave velocities by measuring the arrival time of the observed signal passing through the specimen. The wave propagation time through a specimen can be determined from the analysis of arrival times of the recorded signal.

The *P*-and *S*-wave velocities (V_P and V_S) of the core samples were measured at room P-T conditions using the following relation

Velocity (V) = Length of the specimen (L) /arrival time (δt) (5.5)

The P- and S- wave velocities of the cylindrical cores are measured both in parallel and perpendicular directions to symmetric axis. The parallel and perpendicular directions to symmetric axis correspond to the direction across and along the foliation plane of the core samples. The first recorded travel time (T) of the reference signal is obtained by direct coupling of the transmitter and receiver transducer. Honey is used as acoustic couplant for the measurements of delay time for *P*-and *S*-wave (Fig. 5.15*a*). Similarly, the travel time (t) of test signal is measured by coupling the transducers with the core sample. Thus, the delay time (T-t) is the difference of time measured between the reference signal without sample and test signal with sample. The face-to-face delay time (δt) is estimated for both P-wave and S-wave and it is 21 microseconds and 36.17 microseconds, respectively (Fig. 5.15*b*, *c*).

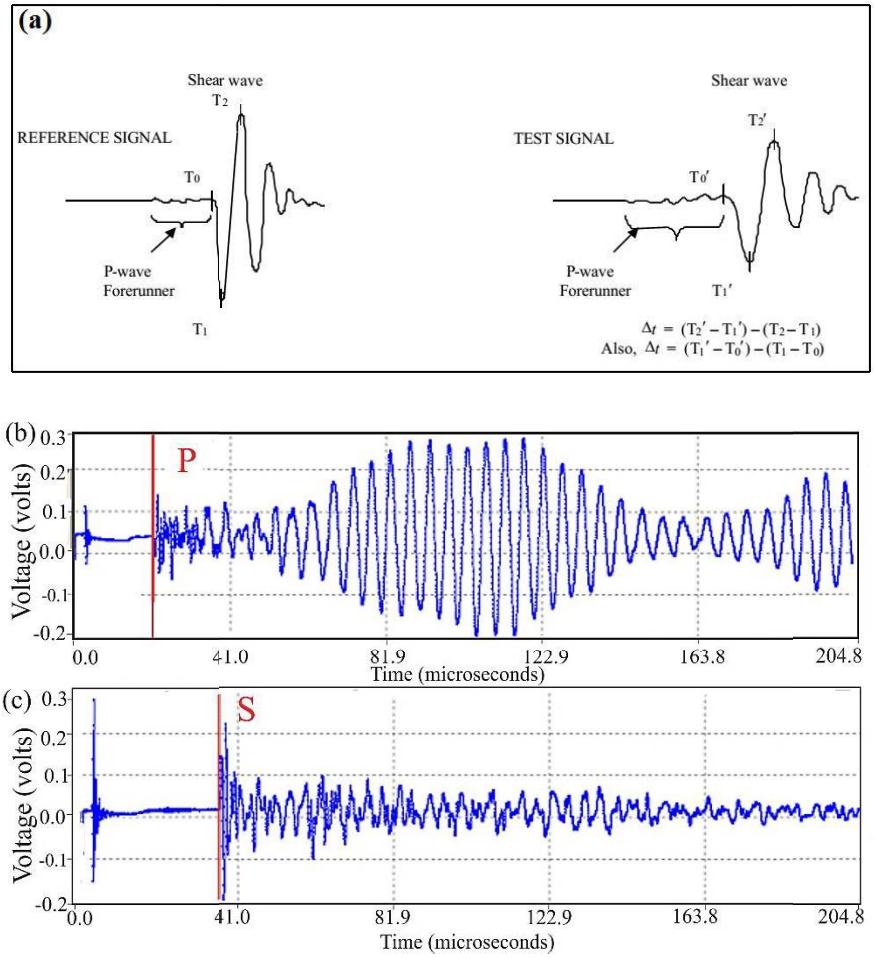

Figure 5.15 (a) The waveforms of reference and test signal for delay time measurement (b) Reference P-wave with delay time is 21 microseconds and (c) reference S-wave with delay time is 36.17 microseconds.

The ultrasonic measurements of seismic velocities are carried out for all cored samples using the transmitter and receiver transducers which are then pasted to both the ends of the core sample. The V_P, V_S and δt were then estimated using eqn. 5.5 and each test was repeated ten times to take an average value of velocities were estimated.

It has been noted that velocity in a rock mass is much higher when measured along the foliation compared to across the foliation. This type of mechanical behaviour of a rock gives rise to seismic anisotropy. Seismic anisotropy can be defined as the difference between the maximum and minimum velocities divided by the average of two respective velocities (Birch, 1961; Thill et al., 1969). The ultrasonic *P*-wave anisotropy coefficient (A_P) is

defined as a function of *P*-wave velocity along ($V_{P\ (along)}$) and across the foliation ($V_{P(across)}$) and Similarly, the ultrasonic *S*-wave anisotropy coefficient (A_S) is defined as a function of measured *S*-wave velocity along ($V_{S(along)}$) and across the foliation ($V_{S(across)}$) and can be expressed as :

$$A_P = V_{P\,(along)} - V_{P\,(across)}/V_{P\,mean} * 100 \qquad (5.6)$$

and

$$A_S = V_{S\,(along)} - V_{S\,(across)}/V_{S\,mean} * 100 \qquad (5.7)$$

where $V_{P\ (along)}$ and $V_{P\ (across)}$ are the ultrasonic P-wave velocity along and across the foliation and $V_{P\ mean}$ is the mean of two observed *P*-wave velocities.

$V_{S\ (along)}$ and $V_{S\ (across)}$ are the ultrasonic S-wave velocity along and across the foliation and $V_{S\,mean}$ is the mean of two observed *S*-wave velocities.

The positive value of anisotropy shows that the velocity along the foliation is maximum than that in across the foliation, whereas the negative value of anisotropy shows the velocity is maximum in across the foliation than in other direction.

5.5.4 ULTRASONIC RESULTS

In the present study, 23 samples were analyzed for the measurement of V_P and *Vs* in both the directions i.e. along and across the foliationas well as for their associated Ap and As and is estimated for all the studied rocks. The average values of these parameters for each core sample are listed in Table 5.4 and the obtained results are described as follows.

(a) Slates

The variation in $V_P$and *Vs* for all slates (S1-S5) core samples are measured and listed in Table 5.4. Within the slates core samples, the S3 exhibits the lowest average *Vp* (2266 m/s) and *Vs* (1261 m/sec) measured along the foliation plane. Similarly, across the foliation, S3 also have low average values of *Vp* (1927 m/sec) and *Vs* (1114 m/sec) (Fig. 5.16 *a*, *b*). It is observed that the variation of seismic velocities is very less. It is found that the *Vp* is varying

from 2266 m/sec to 3459 m/sec along the foliation and 1927 m/sec to 2854 m/sec across the foliation. The *Vs* is varying from 1261 m/sec to 1597 m/sec and 1114 m/sec to 1297 m/sec, along and across the foliation, respectively.

The seismic anisotropy coefficient of seismic velocities (Ap and As) is also measured for all the slates core samples and is listed in Table. 5.4. It is observed that slates cores show lowest anisotropy coefficients (Fig. 5.17). The Ap found to be varying from 16% to 21% and As is varying 12% to 19%.

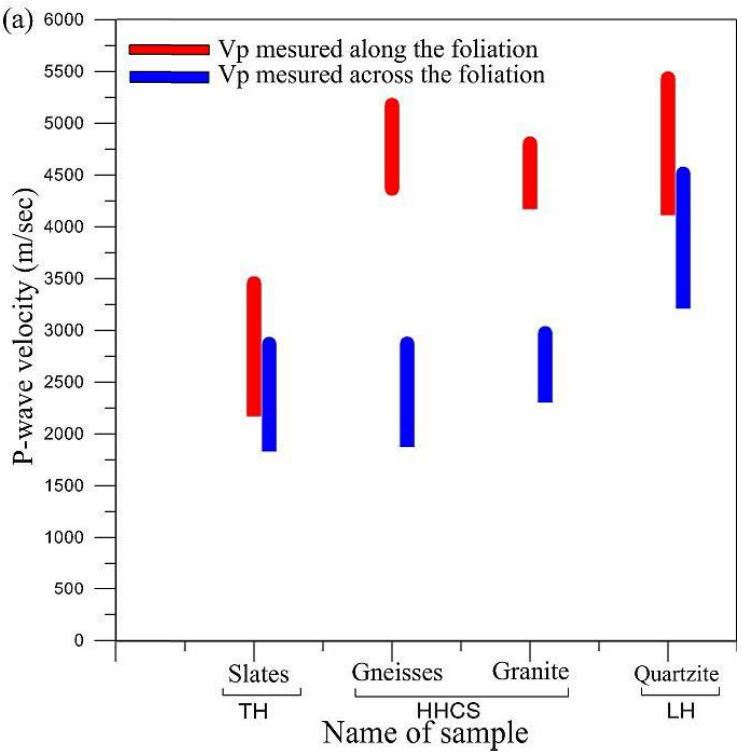

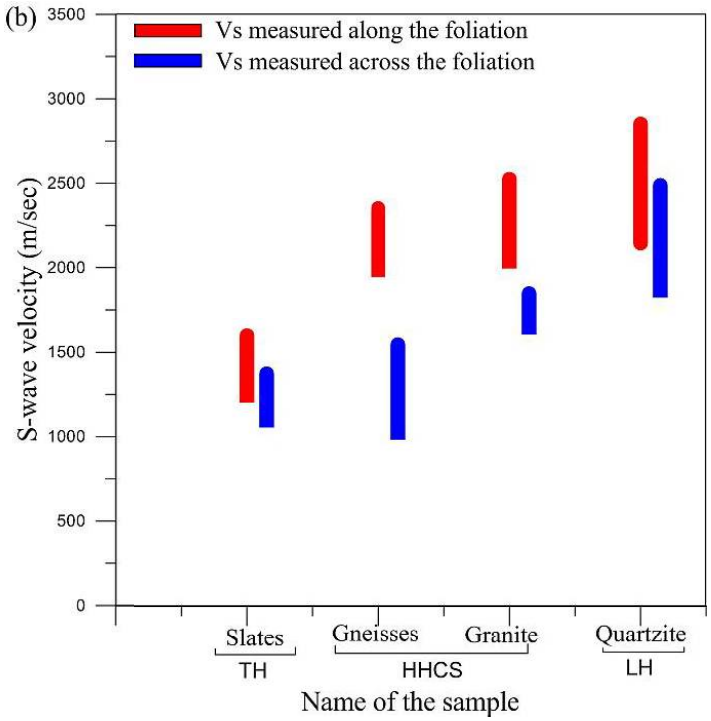

Figure 5.16 Variation in seismic velocities measurementsin slates, gneisses, granites and quartzites (*a*) *Vp* measured along and across the foliation, (*b*) *Vs* measured along and across the foliation

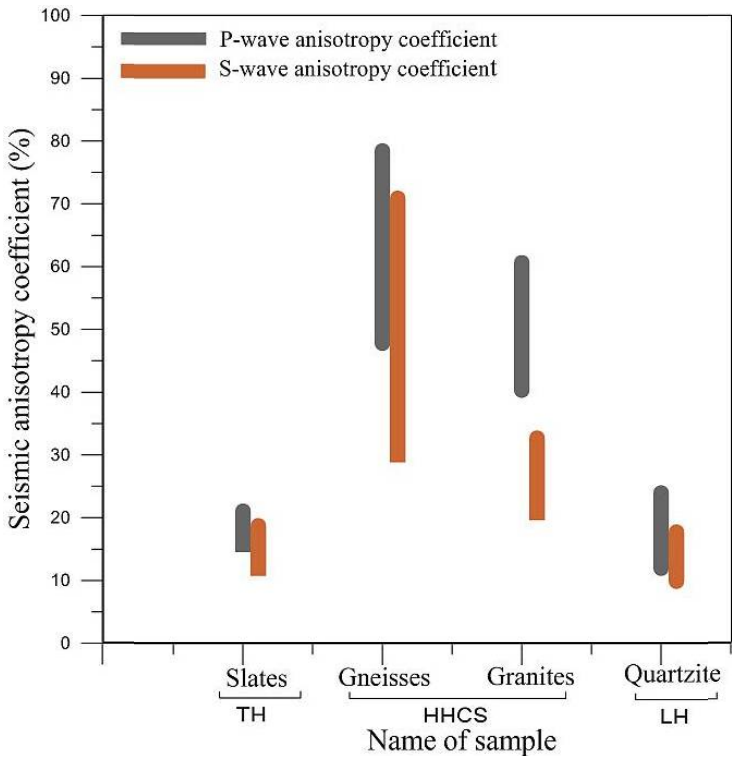

Figure 5.17 Variation of seismic anisotropy coefficient for *P*-wave (Ap) and *S*-wave (As) in slates, gneisses, granites and quartzites.

(b) GNEISSES

The variation of *P*-and *S*-wave velocities for all gneisses (GN1-GN8) are measured and listed in Table. 5.4. It has been observed that the velocities in gneisses are highly variable. The *Vp* is vary from 4370 m/sec to 5181 m/sec and 1973 m/sec to 2879 m/sec measured along and across the foliation, respectively (Fig.5.16 *a*). The *Vs* is found to be varying from 2004 m/sec to 2359 m/sec along the foliation and 1043 m/sec to 1544 m/sec across the foliation (Fig. 5.16 *b*).

The Ap and As measured for all gneisses samples and observed to be higher than granites, quartzites and slates cores and are presented in Table. 5.4. The Ap is varying from 48 to 79 % and As is 30 to 71% (Fig. 5.16).

(c) GRANITES

The granites cores exhibit higher seismic velocities than slates cores as shown in Figure 5.16 (*a*, *b*). All the granites cores exhibit more or less similar average *Vp* ranging between 4267 m/sec and 4811 m/sec and *Vs* ranging between 2059 m/sec and 2529 m/sec, measured along the foliation. An average value of *Vp* and *Vs* observed across the foliation which vary from 2400 m/sec to 2980 m/sec and from 1662 m/sec to 1852 m/sec, respectively (Fig. 5.16 *a*, *b*)

The anisotropy coefficients for both *P*- and *S*-wave of all granites cores are listed in Table 5.4. It has been observed that the average of Ap and As in all granites (G1-G5) is more than the slates (S1-S5). It is varying from 40 to 61% for Ap and 21 to 33 % for As.

Table 5-4 List of average values of seismic wave (*P*-and S-wave) velocities in slates, gneisses, granites and quartzites measuredin both along and across the foliation with their corresponding P- and S-wave anisotropy coefficients.

Sample No.	Rock type	Density (kN/m3)	P-wave Velocity (*Vp*) (m/sec)		S-wave velocity(*Vs*)(m/sec)		Seismic Anisotropy Coefficient	
			Along the foliation	Across the foliation	Along the foliation	Across the foliation	A_P (%)	A_S (%)
S1	Slates (TH)	26.90	3362	2854	1479	1284	16	14
S2		26.90	3433	2877	1597	1373	18	15
S3		27.50	2266	1927	1261	1114	16	12
S4		26.40	3459	2799	1566	1297	21	19
S5		26.00	3392	2848	1371	1180	17	15
GN1	Gneisses (HHCS)	26.40	4370	2378	2290	1332	59	53
GN2		26.70	4772	2879	2068	1337	49	43
GN3		26.80	4526	1973	2189	1043	79	71
GN4		26.40	4563	2029	2068	1521	77	30
GN5		26.70	4861	2836	2004	1341	53	40
GN6		27.10	5181	2510	2359	1544	69	42
GN7		25.05	5085	2478	2123	1167	69	58
GN8		26.00	4577	2805	2073	1423	48	37
G1	Granites (HHCS)	26.70	4483	2980	2485	1850	40	29
G2		26.30	4389	2916	2341	1770	40	28
G3		25.20	4811	2570	2059	1662	61	21
G4		26.70	4267	2400	2529	1819	56	33
G5		25.90	4674	2617	2352	1852	56	24
Q1	Quartzites (LH)	26.30	4578	3869	2855	2493	17	14
Q2		26.30	5436	4272	2464	2075	24	17
Q3		26.40	5051	4214	2236	1955	18	13
Q4		29.10	4205	3309	2253	1885	24	18
Q5		26.70	5096	4521	2151	1948	12	10

(d) QUARTZITES

The *P*-and *S*-wave velocities for all quartzites (Q1-Q5) are observed to exhibit higher *Vp* and *Vs* than slates (S1-S5), granites (GN1-GN8), granites (G1-G5) (Fig. 5.16 *a*, *b*). The *Vp* measured in all the quartzites core samples and it is found that it is vary from 4205 m/sec to 5436 m/sec along the foliation and 3309 m/sec to 4521 m/sec across the foliation (Fig. 5.16 *a*). The *Vs* is found to vary from 2151 m/sec to 2855 m/sec and 1855 m/sec to 2493 m/sec measured along and across the foliation (Fig. 5.16 *b*).

The average values of anisotropy coefficients, Ap and As of all quartzites (Q1-Q5) is listed in Table 5.4 and shown in Figure 5.17. It is noted that these coefficients (Ap and As) are very low as compared to gneisses and granites, but it is slightly higher than slates. For quartzites Ap is varying from 12 to 24% and As is varying from 10 to 18% (Fig. 5.17).

5.6 DISCUSSION

Shear wave splitting is a unique approach that provides significant constraints on the anisotropic properties and deformation characteristics of the crust. The *S*-wave of local and regional earthquakes are most commonly used for studying crustal anisotropy (e.g. Bowman & Ando, 1987; Vavryčuk, 1993; Paulssen, 2004; Teanby et al., 2004; Musumeci et al., 2005), but there are limitations in using local *S*-wave, as it is contaminated with high-frequency noises as well as source effects. Moreover, in regions like the Himalaya, seismicity is mostly confined in the upper crust. Consequently, information of the lower crust cannot be achieved using shallow focus earthquakes. In many studies, the GPS measurements are also used as constraints on the deformation on the earth's surface and even on the shallow crust. However, the GPS study (Jade et al., 2011) cannot provide constraint for the whole crust particularly middle to lower crust. Moreover, focal mechanism data of shallow focus earthquakes cannot provide information on existing stress and deformation in the lower crust. The splitting of *Ps* phase has significant importance in studying crustal anisotropy. As this phase is produced at the Moho discontinuity and reaches vertically to the recording station, thus the travel

path of the wave is confined within the crust only. Moreover, complexities of source time function and contaminations of high- frequency cultural noises are absent in the *Ps* phases; these effects are eliminated during deconvolution process used for computation of RFs. Thus, splitting analysis of *Ps* phase provides unique opportunity to obtain the anisotropic information for the whole section of the crust. The source of anisotropy in the study region and its geodynamic implication in the study region is discussed below.

5.6.1 PRIMARY SOURCE OF SEISMIC ANISOTROPY

The splitting of *Ps* phase could be due to the different origin of anisotropy within the crust somewhere along the propagating path and often it is difficult to ascertain the source of anisotropy. The anisotropy is primarily originated from (i) aligned micro-cracks developed due to tectonic stress - SPO (Crampin, 1984; Crampin & Lovell, 1991) and/or (ii) lattice preferred orientation of middle to lower crustal rocks (Barruol & Mainprice, 1993). The anisotropy due to micro-crack alignment is most commonly inferred in the upper most part of the crust (Crampin, 1981). In a compression tectonic regime, the micro-cracks aligned themselves perpendicular to the force close, and parallel to the force open. Thus, causing the fast polarization directions of the anisotropy caused by the micro-cracks is parallel to the compression force. In NW Himalaya, the compressional force is acting in the NE direction, but the FPDs at most stations do not follow the stress direction. This indicates that contribution of anisotropy induced by upper crustal micro-cracks is insignificant. Moreover, as the homogeneity increases with depth, micro-cracks are far less significant at greater depths (Rasolofosaon et al., 2000). The FPDs and larger strength of anisotropy observed in this study suggests the significant contribution from the middle to lower crust compared to the upper crust. The delay time as high as 0.80 s cannot be caused only by upper crustal micro-cracks, however, the presence of micro-cracks can influence splitting results up to some extent. The crust beneath the study region varies within 50-60 km as reported by RF studies (Hazarika et al., 2014, 2017). For such thick crust, the contribution of anisotropy from the middle and lower crust is much significant compared to the upper part of the crust (e.g. Paul et al., 2017). In

the middle to lower crustal depths, anisotropy can be caused by comparatively large parallel fractures, and/or alignment of mineral fabric or LPO (Araragi et al., 2015). This type of anisotropy is known as intrinsic anisotropy or structural anisotropy. The LPO of anisotropic minerals present in the middle and lower crustal depths are considered as a most possible explanation for anisotropy (Barruol & Mainprice, 1993). Some of the crustal rocks show anisotropy characteristics; mainly phyllosilicates (micas) mineral in upper-middle crust and amphiboles in the lower crust (Christensen & Mooney, 1995). Laboratory experiments (Babuška & Cara, 1991) and petrophysical studies (Barruol & Mainprice, 1993; Weiss et al., 1999) suggest that most of the minerals constituting the bulk of the crust are anisotropic to some extent. The predominant NW-SE orientation of FPDs observed in the present study follows the regional tectonic features rather than the NE oriented GPS velocity vectors (Jade et al., 2011). The distribution of FPDs near and within the active fault zones also favors the directions parallel to the strike of the faults (e.g. MCT/VT and STD).

The FPDs display scattered values at single station and between different stations. The observed wide variation of FPDs at stations e.g. DIGA, HURL, and KAZA may be due to combined effect of anisotropy due to micro-cracks developed owing to tectonic force and also induced by structure (Fig. 5.10). Another source of scattering of FPDs is the interaction of shear wave with the irregular surface or subsurface topography along the propagating path (Crampin & Lovell, 1991). However, the average values of FPDs show consistently NW-SE orientation. The result of the present study is comparable to the reported splitting parameters observed in adjacent LKZ (Paul et al., 2017). The average FPDs at SARA and TAPR follows roughly the strike of the VT (Fig. 5.10). The RACK station, on the other hand, shows NNW-SSE trend following the STD which is N-S oriented near this region. Thus, the FPD follows the local geological structure suggesting structural anisotropy.

5.6.2 EFFECT OF EXTENSION TECTONICS ON SPLITTING PARAMETERS

In the NW Himalaya, ongoing E-W extension has been reported by earthquake focal mechanism solutions (Molnar & Lyon-Caen, 1989; Molnar, 1992) as well as geological (e.g. Epard & Steck, 2008; Thiede et al., 2006) and geodetic study (Banerjee & Burgmann, 2002). Extension tectonics is evidenced in the Leo Pargil Detachment Zone (LPDZ) of Kinnaur Himalaya by both geological and geophysical studies (e.g. Thiede et al., 2006; Yadav et al., 2017; Singh et al., 1975; Khattri et al., 1978). The source mechanism of 1975 Kinnaur earthquake of Ms 6.8 occurred near the Kaurik-Chango Fault shows normal faulting suggesting extension parallel to the Himalayan Arc (Singh et al., 1975; Khattri et al., 1978). Such extensional strain within the crust results in the LPO of anisotropic minerals (Barruol & Mainprice, 1993; Tatham et al., 2008; Weiss et al., 1999). In a compressional regime, the minerals are aligned themselves with the maximum shear stress or tension stress, which is parallel to the extension direction (Ribe, 1992). When shear wave travels through the crust the fast split waves follows the direction of maximum shearing along the extension direction. Thus, the observation of splitting parameters using *Ps* phase provides important insight into the deep crustal response towards extension and deformation. The observation in the study provides support for the assumption that the deep crust within the study region has undergone extensive and relatively uniform strain in response to crustal thinning and extension. The effect of extension tectonics on anisotropy or shear wave splitting has also been reported in Tibetan Plateau and NE China (Sherrington et al., 2004; Guo et al., 2016). In several studies, the evidence of seismic anisotropy has been used for studying deep crustal deformation caused by extension (Moschetti et al., 2010).

5.6.3 SEISMIC ANISOTROPY OF ROCK SAMPLES

Seismic anisotropy is one of the important properties of rocks and is defined by the change in seismic velocity with direction in an anisotropic medium. In rocks, it is mainly due to preferred orientation of certain minerals/

microcracks/ impurities (Christensen, 1984; Siegesmund et al., 1989). In the present study, seismic velocity (both *P*-and *S*-waves) in rocks, along and across foliation have been studied.

The results obtained from laboratory studies of rock samples under normal pressure and temperature conditions, shows that the seismic velocities observed along the foliations are higher than those measured across the foliations. The *Vp* and *Vs* are observed to be higher in the quartzite cores ($V_{P\ along}$: 5436 m/sec, Vs_{along}: 2855 m/sec; $V_{P\ across}$: 4521 m/sec, $V_{S\ across}$: 2493 m/sec) as compared to granites ($V_{P\ along}$: 4811 m/sec, Vs_{along}: 2529 m/sec; $V_{P\ across}$: 2980 m/sec, $V_{S\ across}$: 1852 m/sec) and gneisses ($V_{P\ along}$: 5181 m/sec, Vs_{along}: 2359 m/sec; $V_{P\ across}$: 2879 m/sec, $V_{S\ across}$: 1544 m/sec), whereas it is lowest in the slates $V_{P\ along}$: 2266 m/sec, Vs_{along}: 1261 m/sec; $V_{P\ across}$: 1927 m/sec, $V_{S\ across}$: 1114 m/sec). Further quartzites and slates exhibit lower anisotropy coefficient for both *Vp* and *Vs*. The quartzites, being mono-mineralic, show the lowest seismic anisotropy coefficient (A_P: 12%; A_S: 10%) indicating its isotropic nature. The gneisses which are highly banded, folded and foliated show high coefficient of anisotropy (A_P: 79%; A_S: 71%) signifying its anisotropic nature, whereas slates are observed to have less developed fracture/foliation and hence have low percentage of anisotropy coefficient (A_P: 16%; A_S: 12%). The granitic and gneisses of HH are having well developed fabric/foliation, and are polymineralic rocks. Thus, these core samples have high value of anisotropy coefficients.

One of the objectives of this study was to access the seismic anisotropy of the Himalayan accretionary wedge and underlying Indian basement rocks. The shear wave splitting analysis enables us to quantify the seismic anisotropy of the whole crust that encompasses both the wedge and the basement that lies below the decollement (MHT). However, one disadvantage of RF analysis is its inability to precisely constraints seismic anisotropy of uppermost crust. Since, the depth profile of the study area can be divided into the Himalayan wedge and the underlying basement rocks. The anisotropy of these units, separated by the MHT, need not to be identical. Apart from this, it also needs to be considered, that measurement of seismic anisotropy in laboratory conditions are performed at room P-T conditions, while the seismic anisotropy

measured through RF methods of the whole crust would have varying and elevated P-T conditions in accordance with the depth at which a given lithology is present. It is tried to correlate the strength of anisotropy observed from delay times (δt) of shear wave splitting (Table 5.3) and anisotropy coefficients (Ap and As) (Table 5.4) obtained in laboratory analysis of rock samples. Both the studies show similar strength of anisotropy in the Higher and Lesser Himalaya, whereas a difference is observed in the TH where anisotropy coefficients is lower in comparison to larger delay time observed in shear wave splitting study.